Reprinted from *Mineral and Rock Deformation: Laboratory Studies—The Paterson Volume*
Geophysical Monograph 36

COMPLETE FABRIC ANALYSIS OF SOME COMMONLY OBSERVED QUARTZ C-AXIS PATTERNS

S. M. Schmid and M. Casey

Geologisches Institut, ETH-Zentrum, CH8092 Zürich, Switzerland

Abstract. The results of a complete fabric analysis based on naturally deformed quartzites suggest that slip in the crystallographic <a> direction dominates over other possible slip directions. Slip on the first order prisms, the positive and negative rhombs, and the basal plane are inferred from the fabric analysis. Unequal slip activity on positive and negative rhombs is interpreted to be primarily responsible for the preferred orientation of these forms. With the help of a calculation of the orientation distribution function (ODF) we propose an interpretation of pole figures for the c- and a-axes in terms of active slip systems, the type of finite strain and the kinematic framework. A consideration of the mechanisms of lattice reorientation suggests that both inhomogeneous deformation and syntectonic recrystallization play an important role in establishing favoured crystal orientations for easy slip in progressive deformation.

Introduction

In principle the analysis of crystallographic preferred orientations (referred to as fabric in this contribution) is of considerable interest for the structural geologist. This is because fabric development is governed by the following three factors: (1) the active deformation mechanisms, (2) the shape of the finite strain ellipsoid (oblate, prolate, plane strain) and to some extent also the strain magnitude and (3) the strain path or kinematic framework (a short discussion may be found in Schmid 1982). The influence of these factors on the fabric of quartz rocks has been well demonstrated by the work of Lister and co-authors [Lister et al., 1978; Lister and Paterson, 1979; Lister and Hobbs, 1980], who were able to carry out computer simulations of fabric development in quartz during plastic deformation based on the Taylor-Bishop-Hill model. It should be theoretically possible to go in the other direction and deduce the role of the three above mentioned factors during deformation on the basis of the measured fabric. What makes the fabric interpretation very difficult is the fact that all these main factors contribute together to the final pattern of the fabric and it is extremely difficult to isolate the influence of each of the them.

The difficulty in the interpretation of fabrics could be partly overcome by more work in experimental rock deformation. In the case of quartz valuable information is available from the work of Tullis et al. [1973] and Green et al. [1970]. The limitation of this experimental information lies in the facts that classical rock deformation experiments produce only oblate strain ellipsoids and that the strain path is extremely simple (co-axial flattening). For technical reasons it is very difficult to investigate experimentally the influence that a different type of finite strain and a different strain path (e.g. simple shear) might have on the resulting fabric.

A second approach to the problem is that chosen by Lister and co-workers [Lister et al., 1978] and by Etchecopar [1977]: a numerical simulation of fabric development based on a particular physical model. The models used for this simulation work have to be simple and somewhat remote from reality. Their direct applicability to nature is limited.

In this contribution we make an attempt to interpret quartz fabrics empirically by making use of the insights gained from experimental and simulation work. The idea is to carry out complete fabric analyses by means of very tedious X ray work, because the information on one crystal direction only, namely the c-axis which can be more readily measured on a universal stage, is too restricted. We will show, with the help of this additional information on other crystal directions, how the understanding of c-axis patterns can be improved.

Complete fabric analyses for particular c-axis patterns are already available from the work of Baker and Wenk [1972], Bunge and Wenk [1977], Riekels and Baker [1977], Bouchez et al. [1979] and Schmid et al. [1981b]. In this contribution ten representative specimens were selected for discussion. They are chosen out of a much larger number of specimens so far analysed in our laboratory.

TABLE 1. List of reflections used for the pole figure data.

peak number	d-spacing (Å)	crystalographic plane	orientation of plane normals colatitude (°)	longitude (°)	intensity contribution (%)
1	4.26	$10\bar{1}0$ m	90.0	0.0	100
2	3.343	$10\bar{1}1$ r	51.8	0.0	70
		$01\bar{1}1$ z	51.8	60.0	30
3	2.458	$11\bar{2}0$ a	90.0	30.0	100
4	2.282	$10\bar{1}2$	32.5	0.0	17
		$01\bar{1}2$	32.5	60.0	83
5	2.237	$11\bar{2}1$	66.0	30.0	100
6	1.980	$20\bar{2}1$	68.5	0.0	33
		$02\bar{2}1$	68.5	60.0	67
7	1.817	$11\bar{2}2$	47.5	30.0	100
8	1.541	$21\bar{3}1$	73.4	19.1	53
		$12\bar{3}1$	73.4	40.9	47
9	1.288	$10\bar{1}4$	17.7	0.0	22
		$01\bar{1}4$	17.7	60.0	78

Measuring Technique and Data Analysis

The pole figures for nine reflections were measured with an automatic X ray texture goniometer operating in combined reflection and transmission mode [Siddans, 1976]. The list of reflections used and the relative intensity contributions of positive and negative forms with the same d-spacing used for the calculation of the ODF are given in table 1. Quartz has a point group symmetry of 32, but due to Friedel's law it has a diffraction symmetry $\bar{3}$m. In a powder diffraction pattern, however, the apparent symmetry is 6/mmm. Knowledge of the structure factors [Smith and Alexander, 1963], nevertheless, allows the calculation of an ODF and of inverse pole figures with the symmetry $\bar{3}$m [Baker et al., 1969]. Separate pole figures for positive and negative forms (figures 4 and 5) can be calculated from the coefficients of the series expansion of the ODF although the measured pole figures result from the contributions of both positive and negative forms [Casey, 1981].

The pole figures were measured in a step scan with 5° intervals in both the angle of tilt and of azimuth. A total measuring time of about 24 hrs. was invested for each pole figure.

Not all the specimens analysed are monomineralic. In the case of specimens R 405 Gran 133, and Gran 125 all minerals other than quartz were dissolved from a thin section using a silica saturated hydrofluoric acid [Kerrich and Starkey, 1979] in order to remove all diffraction peaks other than those of quartz. This section was then used for both transmission and reflection scans.

For the data processing a set of computer programs described by Casey [1981] was used. The calculation of the ODF follows the mathematical methods outlined by Bunge [1969] and the reader unfamiliar with the data presentation in the form of an ODF is referred to Bunge [1969] and Bunge and Wenk [1977] for an extensive description and to Schmid et al. [1981a] for a short introduction. The convention of Euler angles used is that described in Casey [1981].
The specimen reference system has the X-axis perpendicular to the foliation and Z in the folia-

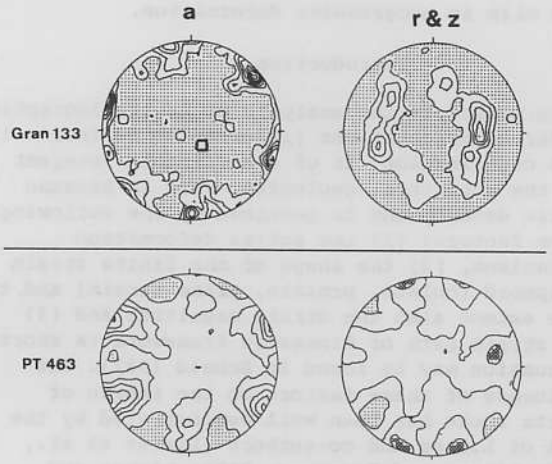

Fig. 1. Measured pole figures for the second order prisms a ($11\bar{2}0$) and the combined reflections from positive and negative rhombs r ($10\bar{1}1$) and z ($01\bar{1}1$) respectively. Since specimen Gran 133 is polymineralic it represents an example of data with a relatively poor quality. PT 463 is a representant of high quality data obtained with monomineralic material. The contour intervals are at 1.0 (Gran 133) and 0.5 (PT 463) in terms of a uniform distribution. Stippled areas have a density of less than 1.0 and 0.5 respectively.

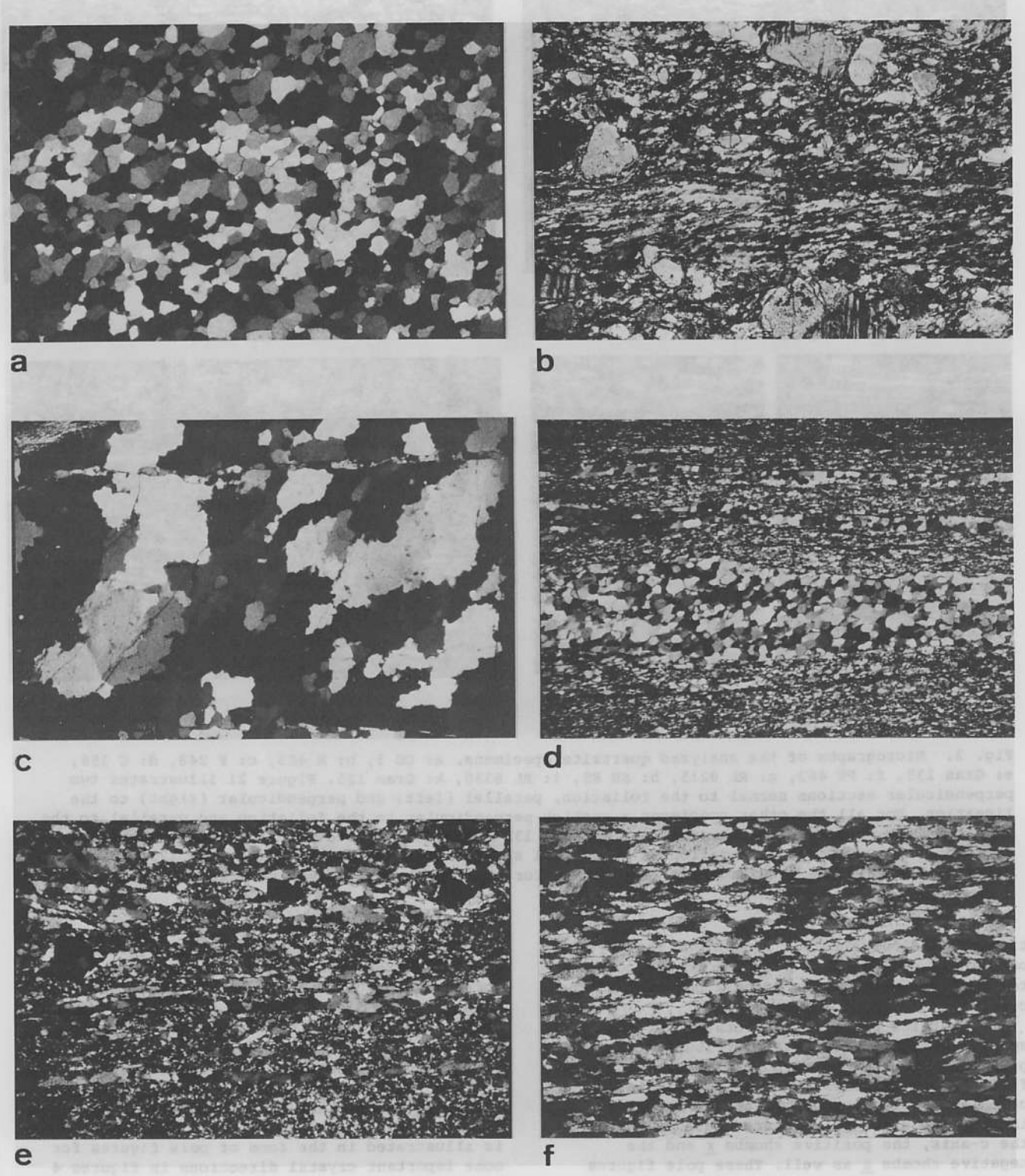

Fig. 2. For legend see next page.

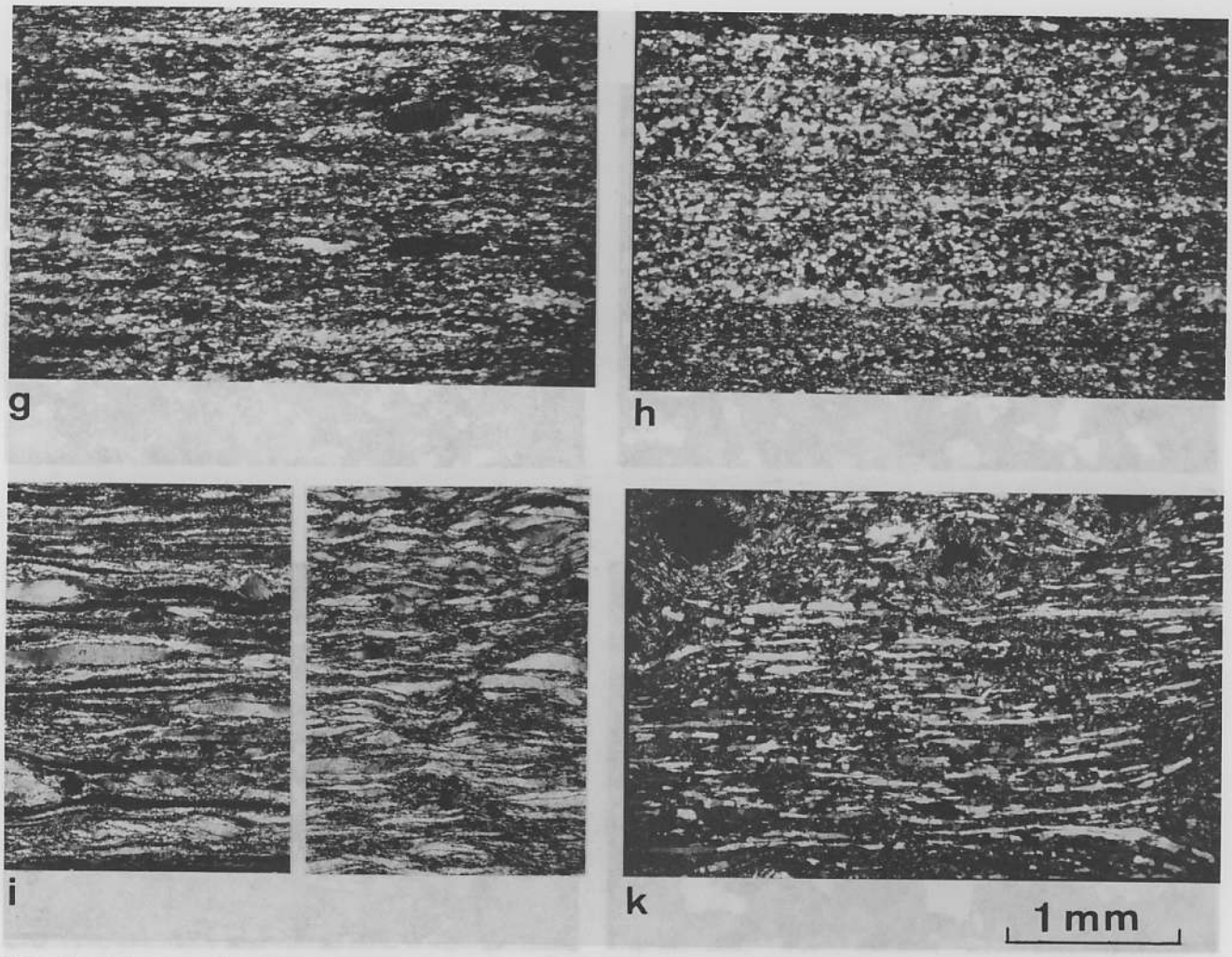

Fig. 2. Micrographs of the analysed quartzite specimens. a: CC 1, b: R 405, c: P 248, d: C 156, e: Gran 133, f: PT 463, g: RL 8215, h: SE 85, i: RL 8330, k: Gran 125. Figure 2i illustrates two perpendicular sections normal to the foliation, parallel (left) and perpendicular (right) to the lineation. For all the other specimens a section perpendicular to the foliation and parallel to the lineation was chosen, with the exception of Gran 133 (perpendicular to the lineation). Where the rotational component of deformation is known (all specimens except Gran 133 and Gran 125) the movement sense is dextral. The magnification is the same for all micrographs (given next to figure 2k).

tion perpendicular to the lineation. The crystal coordinate system has X parallel to the normal to the first order prism m and Z parallel to the c-axis.

The lattice preferred orientation of the specimens analysed in this contribution is presented in the form of pole figures calculated from the ODF (figures 4 and 5). We display calculated pole figures because we intend to include important pole figures such as those for the c-axis, the positive rhombs r and the negative rhombs z as well. These pole figures cannot be measured but they can be calculated from the ODF. Figure 1 displays measured pole figures for two selected specimens: Gran 133 (low quality data) and PT 463 (high quality data). A direct comparison with the corresponding calculated pole figures found in figures 4 and 5 demonstrates excellent agreement between measured and calculated pole figures.

Geological Setting and Microstructure

The microstructure of the specimens described below is illustrated in figure 2 and their fabric is illustrated in the form of pole figures for some important crystal directions in figures 4 and 5. All the micrographs are oriented in accordance with the pole figures, i.e. the foliation aligned East-West and they all represent X-Z

Fig. 3. Polished section through a shear zone from Cap de Creus, Spain. Size, location and reference frame for specimen CC 1 are indicated by the inserted frame. Also indicated are the shear zone boundary (solid line) and the trace of the foliation (dashed line).

sections with the exception of specimen Gran 133 cut in the Y-Z section. In the case of specimens deformed in shear, the shear sense is dextral for both the micrographs (figure 3) and the pole figures (figures 4 and 5).

Specimen CC 1.

A mylonitized quartz vein from Cap de Creus (Spain) is embedded in cordierite-andalusite grade schists. Both schists and veins are affected by shearing under greenschist facies conditions [Carreras et al. 1977]. Figure 3 illustrates the shear zone on the scale of a hand specimen from which CC 1 was selected. The geometry of the sheared quartz vein suggests a strain path closely approximating that of simple shear. The shearing strain can be estimated to vary between $\gamma = 3.2$ and 6.2 within the analysed specimen (figure 2). White et al. [1978] carried out TEM work on similar material from Cap de Creus. Optically determined c-axis pole figures on material from this area have been published by Garcia Celma [1982] and a complete fabric analysis of a specimen from the area is found in Schmid et al. (1981b, specimen CC 627). The microstructure is characterized by nearly equant grains with well equilibrated grain boundaries (grain size around 100μm). Syntectonic recrystallization by the subgrain rotation mechanism went to completion in the centre of the shear zone, although some globular quartz porphyroclasts survived in the low strain region of the hand specimen (figure 3).

Specimen R 405.

A 1-2 mm wide quartz rich band formed in the centre of a shear zone affecting a pegmatitic vein in the late Hercynian granodiorite from the Rosas area (Spain). For additional information see Simpson et al. [1982] and Simpson [1983]. The shear zone formed under lower greenschist facies conditions and the feldspars deformed brittlely. The quartz band illustrated in figure 2b is oriented at about 12° to the shear zone boundary and the East-West line in the pole figures (figure 4) refers to the orientation of this quartz-rich band. Assuming the orientation of the quartz band to approximate the plane of finite flattening, a shear strain of $\gamma = 4.5$ can be inferred. The quartz grains are undulose, exhibit sutured grain boundaries and elongate subgrains and recrystallized grains with a grain size of 20-50μm formed. The long axes of these new grains are aligned at 25-30° to the orientation of the quartz-rich band in accordance with the known sense of shear [Simpson and Schmid, 1983].

Specimen P 248.

A syntectonically recrystallized quartz vein is embedded in a mylonitic quartzo-feldspathic gneiss from the Koralpe in the Autroalpine nappes of eastern Austria (the so-called "Plattengneiss", Frey 1984). This gneiss underwent a shearing deformation under amphibolite facies conditions and it exhibits a very strong North-South trending stretching lineation. Optical measurements of the c-axis orientation indicate that the quartz fabric in the quartz vein is identical to that in the country rock. The microstructure indicates syntectonic recrystallization by grain boundary migration associated with grain growth, leading to a wide spectrum of grain sizes (30-1000μm).

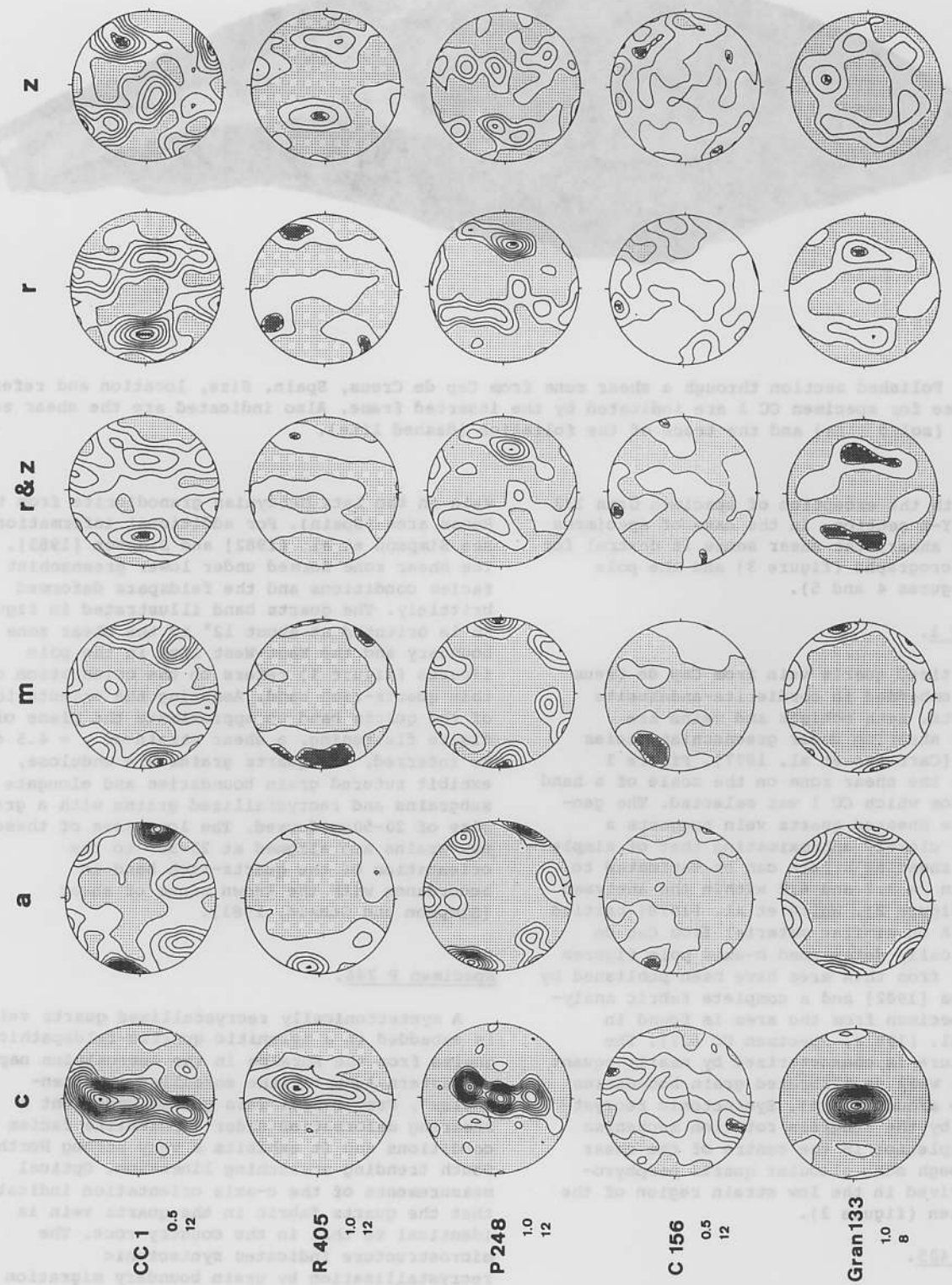

Fig. 4. For legend see figure 5.

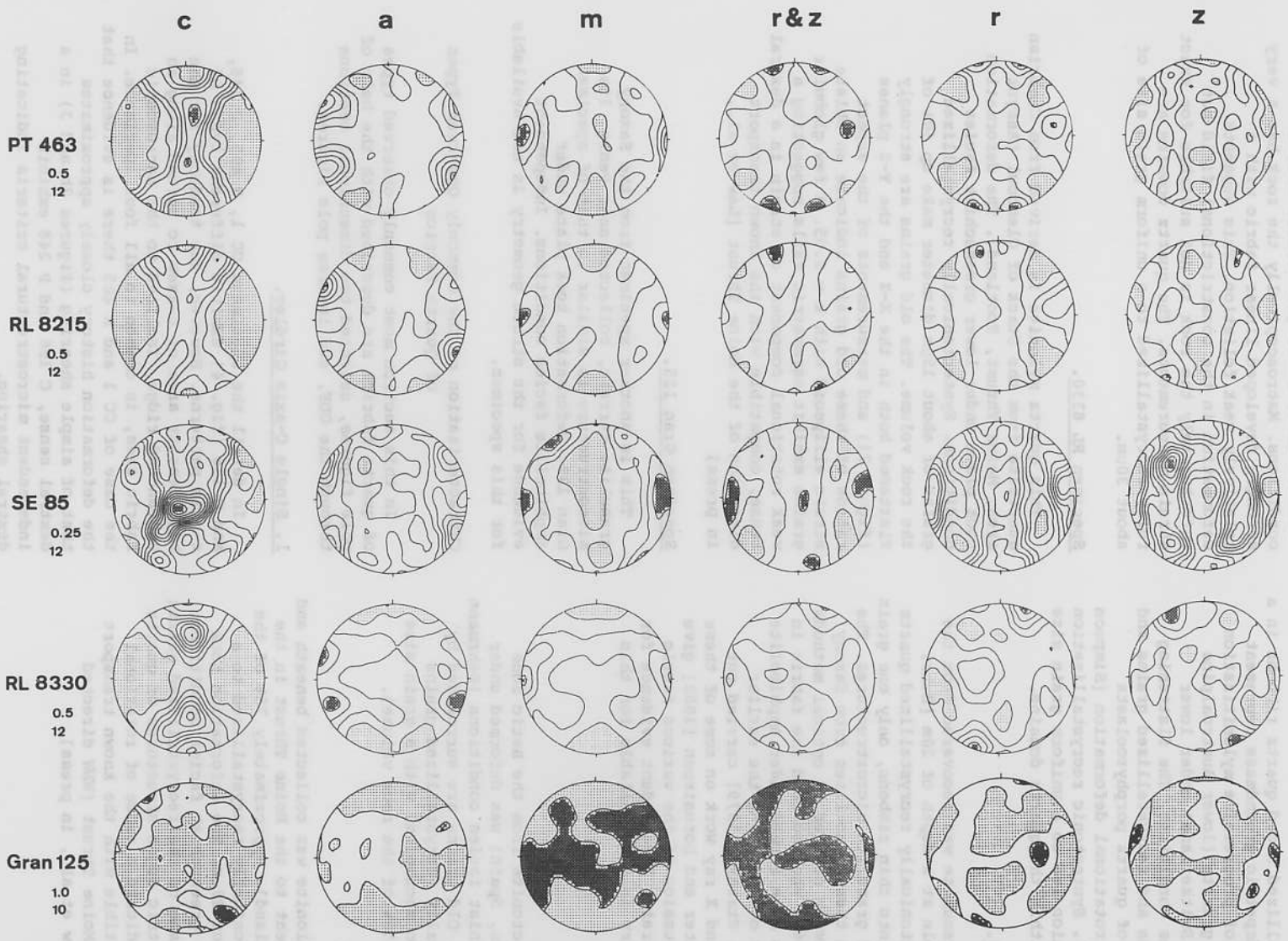

Fig. 5. Pole figures of the c-axis (c), second order prisms (a), first order prisms (m), combined positive and negative rhombs (r+z), positive rhombs (r), and negative rhombs (z). All pole figures calculated from the ODF. The contours are given in multiples of a uniform distribution, the contour interval is 0.25, 0.5 or 1.0, and the order of expansion used for the calculation of the pole figures is 8, 10 or 12 (see the figures listed below the specimen label). Stippled areas have a density of less than 0.25, 0.5, or 1.0 respectively, and crosshatched areas represent areas of maximum density. In general the specimen reference frame is such that the foliation normal is N-S and the lineation E-W. For specimen CC 1 the reference frame is indicated in figure 3, and for R 405 the quartz-rich band shown in figure 2b is E-W. Where the rotational component of deformation is known (all specimens except Gran 133 and Gran 125) the movement sense is dextral.

Specimen C 156.

Fully recrystallized broad quartz ribbons in a fine-grained feldspathic groundmass represent the end products of progressive mylonitization of the Corvatsch granite (lower Austroalpine nappes, Engadin, Switzerland) under lower greenschist facies conditions. The flattening plane of subgrains and recrystallized grains and asymmetric tails of quartz porphyroclasts clearly indicate rotational deformation [Simpson and Schmid, 1983]. Syntectonic recrystallization by subgrain rotation led to a uniform grain size of around 50μm within the quartz domains.

Specimen Gran 133.

This Saxony granulite was recovered from the Tirschheim borehole at a depth of 20m [Behr, 1965]. The syntectonically recrystallized quartz is concentrated into thin ribbons, only one grain broad, typical of granulite microstructures. The quartz fabrics in these granulites from Saxony have been extensively studied by optical methods by Behr [1961, 1965] who ascribed the fabric in the granulites to have formed under amphibolite facies conditions overprinting the earlier granulite facies. Starkey [1979] carried out further optical and X ray work on some of these specimens and Lister and Dornsiepen [1982] give an extensive discussion of the various fabric types in this terrain. Independent evidence for the strain geometry is not available for this specimen.

Specimen PT 463.

This quartz tectonite from the Betic Zone (Betic Cordilleras, Spain) was deformed under lowermost greenschist facies conditions [Behrmann and Platt, 1982]. Old grains are surrounded by small syntectonically recrystallized grains (subgrain rotation mechanism) with a grain size of around 20μm. (50% of the rock volume).

Specimen RL 8215.

This quartz mylonite was collected beneath and immediately adjacent to the Moine Thrust in the Assynt area (Scotland). Approximately 75% of the volume is syntectonically recrystallized to a grain size of about 20μm. The deformation took place under lower greenschist facies conditions. The flattening plane of the recrystallized quartz grains and asymmetric augen structures of quartz porphyroclasts indicate a sense of rotational deformation compatible with the known transport direction of the Moine Thrust (WNW directed overthrusting, Law et al., in press).

Specimen SE 85

This mylonite from the Insubric Line (Val d'Ossola, Italy), is derived from quartzo-feldspathic meta-sediments (Canavese) deformed under lower greenschist facies conditions. Macroscopically the rock has a very strongly developed linear fabric with a relatively weak foliation. This suggests deformation in the constrictional field but unfortunately the rock is not suitable for exact strain measurements. The quartz domains are fully recrystallized to a uniform grain size of about 30μm.

Specimen RL 8330.

This quartz mylonite is derived from Cambrian quartzite from the Stack of Glencoul (Assynt area, Moine Thrust, Scotland). The deformation took place under lower greenschist facies conditions. Syntectonically recrystallized grains of about 15μm diameter make up 60% of the rock volume. The old grains are strongly flattened both in the X-Z and the Y-Z planes (figure 2i) and measurements of the aspect ratios of these old grains indicate an oblate strain ellipsoid with k = 0.05. A few globular grains exhibit asymmetric tails suggesting a weak rotational component of strain in a dextral sense, compatible with the known transport direction of the Moine Thrust [Law et al., in press]

Specimen Gran 125.

This is another specimen from the Saxony granulite terrain, collected near Penig. Its microstructure is similar to that of specimen Gran 133. Deformation took place under amphibolite facies conditions. Independent evidence for the strain geometry is not available for this specimen.

Characterization of the Commonly Observed Types of Quartz Fabrics

In this section most commonly observed types of quartz fabrics are described with the help of pole figures, selected two dimensional sections through the ODF, and inverse pole figures.

1. Single C-axis Girdles.

In detail the specimens CC 1, R 405, P 248, and C 156 (fig. 4) exhibit different types of c-axis patterns. However, the tendency for the high density area of c-axes to spread along an unbranched ridge, inclined to the macroscopic fabric axes, is common to all four specimens. In the case of CC 1 and R 405 there is evidence that the deformation history closely approximates that of simple shearing (figures 2b and 3) in a dextral sense, C 156 and P 248 exhibit independent microstructural criteria indicating dextral shearing.

In spite of substantial differences in the c-axis patterns, the a-pole figures for the four

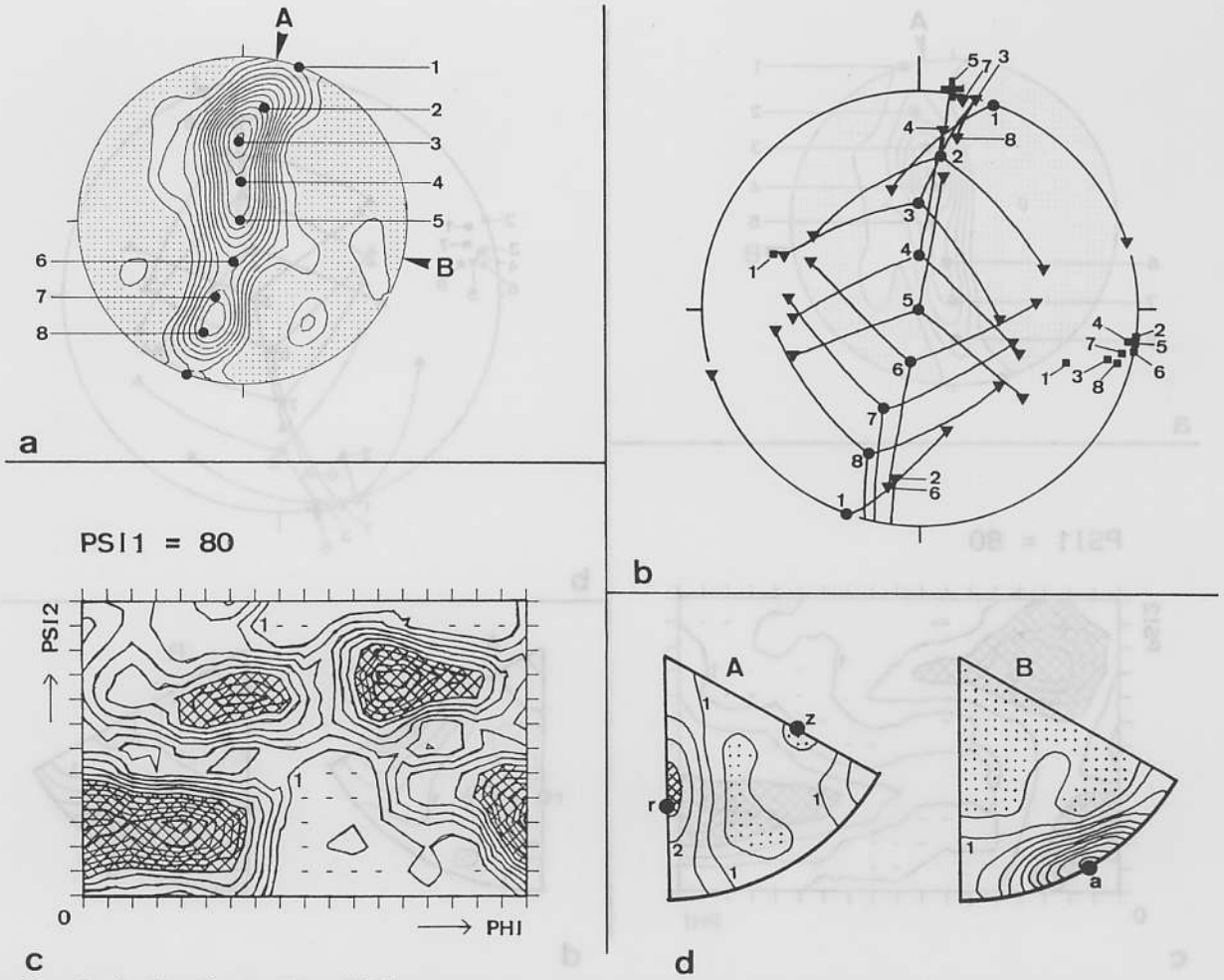

Fig. 6. Analysis of specimen CC 1.
a: Pole figure for the c-direction (contour interval 1.0) indicating and numbering the c-axis positions of crystal orientations chosen for the construction in figure 6b. Specimen directions A (normal to the shear plane) and B (shearing direction) were used for the calculation of the inverse pole figures shown in figure 6d.
b: Favoured crystal orientations for selected c-axis positions shown in figure 6a. Dots: c-axis; triangles: poles to the positive rhombs; squares: one of the three <a> directions, closely aligned with the B specimen direction; cross: pole to the first order prism of c-axis position 5.
c: Section through the three-dimensional graphical representation of the ODF. Order of expansion: 10; contour interval: 1.0. Dashes indicate crystal positions with probabilities calculated to be negative. Crosshatched area: probability higher than 6.0.
d: Inverse pole figures for the specimen directions A and B (see figure 6a). Order of expansion: 12; contour interval: 0.5. A crystal projection with the c-axis in the centre was chosen, and the positions of the r, z and a-directions are indicated.

specimens are strikingly similar (figure 4). A strong a-axis maximum at the margin of the pole figure is situated at an angle of less than 30° to the East-West direction, whereas the preferred orientation of the first order prisms m is more diffuse, especially in the case of CC 1 and R 405. For specimen CC 1 the angle of 12° between the strongest a-axis maximum and the East-West direction is very close to the angle of 10° measured between the inferred shear zone boundary and the same East-West direction (figure 3). In the case of R 405 an angle of 9° was measured between the a-axis maximum and the East-West reference line of the pole figure (parallel to the quartz-rich band, figure 2b), close to the angle of 12° measured between the shear zone boundary and this same reference line. Thus, in the case of both these specimens the a-axis maximum is oriented parallel to the shear zone boundary, within the measuring

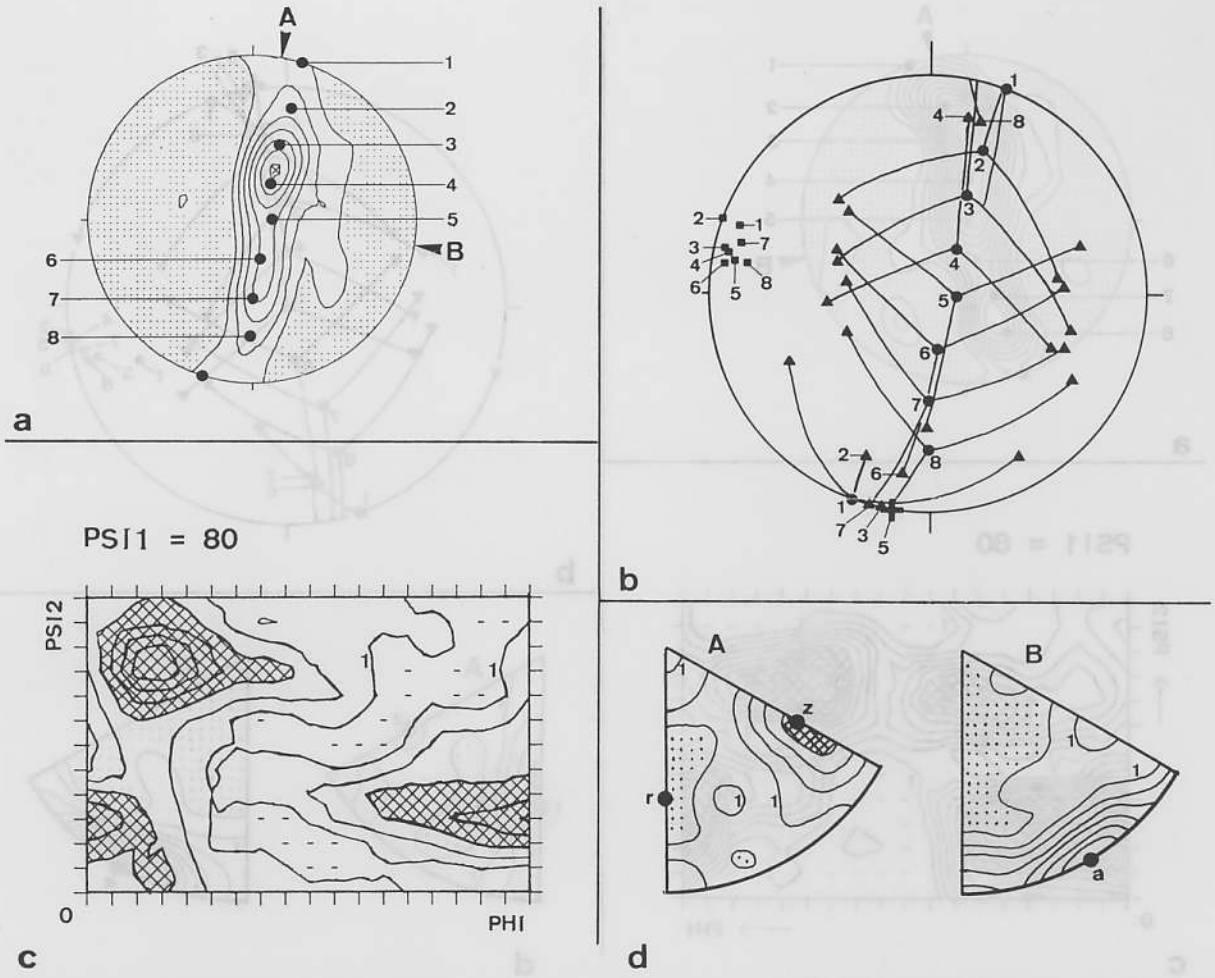

Fig. 7. Analysis of specimen R 405. For reading figures a,b,c, and d see the figure captions for the analogous figure 6, except that figure 7a utilizes a contour interval of 1.0, and that figure 7b indicates the positions of the normals to the negative rhombs z.

errors. During heterogeneous simple shear only displacements parallel to the shear zone boundary and in the shearing direction are allowed and thus we can conclude that there is a preferred alignment of a-axes parallel to the shearing direction in the rock.

In order to know more about the orientations of crystallographic directions other than c and <a>, eight particular c-axis positions along the skeletal line [Lister and williams, 1979] of the single c-axis girdle were selected for specimens CC 1 and R 405 (figures 6a and 7a) and the most probable (favoured) positions of the poles to the positive rhombs r (figure 6b) and the negative rhombs z (figure 7b) were plotted on a stereogram.

This analysis in terms of favoured crystal positions is based on looking at a series of cuts through the three dimensional representation of the ODF [Bunge, 1981, Casey, 1981]. Two such cuts are presented in figures 6c and 7c: the particular cuts at PSI 1 = 80° were purposely chosen because they contain all the information for such crystals which position their c-axes on a great circle inclined by 10° to the North-South line in the pole figure in a clockwise sense (i.e. on a great circle whose pole is at 80° away from the North-South line in a counterclockwise sense; for the convention of Eulerian angles used in this analysis see Casey, 1981 and for some examples see Schmid et al., 1981b). The angles PSI 1 and PHI locate the c-axis, and the third angle PSI 2 determines the location of other crystal directions via a rotation around the final position of the c-axis from 0° to 120° (trigonal symmetry). Sometimes two equally strong maxima at 60° separation are found along such a traverse and we will later refer to such a fabric as having a hexagonal character. In other cases there is only one maximum or two unequal maxima (trigonal character). At PHI = 0° or 180° the c-axis is

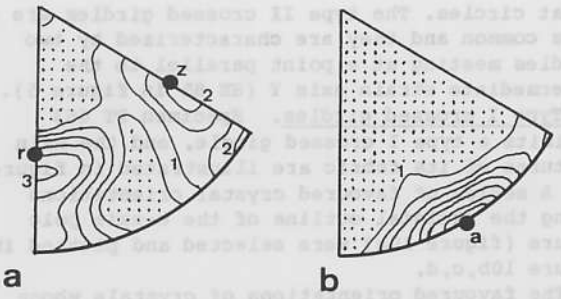

Fig. 8. Inverse pole figures for specimen P 248.
a: Inverse pole figure for the inferred shear plane normal; contour interval: 0.5.
b: Inverse pole figure for the inferred shearing direction; contour interval: 1.0.

located in the centre of the pole figure, the angular range in PHI between 0° and 90° covers all the c-axis positions in the northern hemisphere, and the range between 90° and 180° covers the c-axis positions in the southern hemisphere of the pole projection. It can be seen from figure 6c that a strong ridge extends from PHI = 0°, PSI 2 = 30° towards PHI = 60°, PSI 2= 30°. Thus, within that portion of figure 6c one particular angle in PSI 2 is favoured (trigonal character). In the case of specimen R 405 (figure 7c) angles of PSI 2 around 90° are favoured within the same range in PHI (0° to 60°). The favoured crystal positions in figures 6b and 7b simply represent the maxima in such a profile parallel to the PSI 2 axis in a cut through the ODF.

Figure 6b indicates a tendency for <a> directions to align with the shearing direction at an angle of about 10° to the East-West direction, a piece of information already obtained from looking at the a-axis pole figure. In addition to this, figure 6b clearly shows the tendency for the poles to the basal plane (position 1), one of the poles to the positive rhombs r (positions 2-4, 6-8) or one of the poles to the first order prisms (position 5) to align close to the normal to the shear zone boundary (position A in figure 6a).

Figure 7b is very similar to figure 6b except that the poles to the negative rhombs z now have this tendency to align with the shear plane normal. An alternative way of looking at the contrast between specimens CC 1 and R 405 is to look at the inverse pole figures for the positions A and B (shear plane normal and shearing direction, figures 6d and 7d): In both cases the shearing direction is preferentially aligned with an a-axis. The shear plane normal is strongly aligned with the positives rhombs in the case of CC 1 and the negative rhombs in the case of R 405. The maxima for the shear plane normal spread towards the c-axis and the poles to the first order prisms m.

The analogous inverse pole figures for specimens P 248 and C 156 are shown in figures 8 and 9 (calculated for specimen directions parallel and perpendicular to the a-axis maximum in analogy to positions A and B in figure 6a). Specimen P 248 shows a tendency for both positive and negative rhombs to align with the inferred shear plane, and the probability of finding a first order prism m aligned with the shear plane is also high. Specimen C 156 on the other hand shows a tendency for the basal plane to align with the inferred shear plane.

A complete fabric analysis on a deformed quartzite from the Main Central Thrust in the Himalaya was carried out by Bouchez et al. [1979]. Their specimen 620 has a fabric almost identical to that of CC 1. Bunge and Wenk [1977] calculated an ODF on two specimens (their specimens Sci 638 and Sci 690 from the Suretta nappe, higher Pennine nappes of eastern Switzerland) which have a fabric very similar to that of our specimen C 156. These specimens were also deformed under lower greenschist facies conditions. In general, references to optically measured single girdles of c-axes are very numerous and only a few are cited here: Bouchez and Pecher [1981], Burg and Laurent [1978], Eisbacher [1970], Garcia Celma [1982], Laurent and Etchecopar [1976], Simpson [1980]. The common feature of these single c-axis girdles is that they are asymmetric in relation to the macroscopic fabric axes.

2. C-axis Point Maxima Parallel to the Intermediate Strain Axis (Y-maximum).

Specimen Gran 133 in figure 4 is representative of this particularly simple fabric. Its character has already been described by Schmid et al. [1981b] and its main features are: (1) A single c-axis maximum parallel to the Y-axis with a tendency to spread along the Y-Z plane; (2) Three a-axis maxima, suggesting a "single crystal" orientation at first sight, with the a-axis maxima asymmetrically disposed

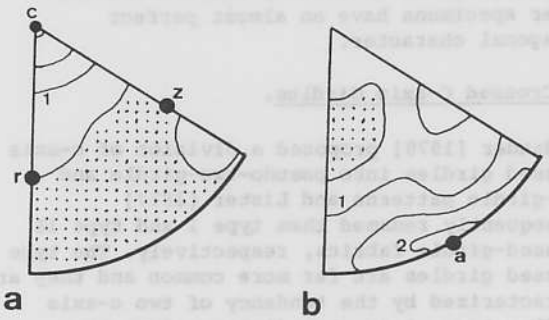

Fig. 9. Inverse pole figures for specimen C 156. Contour interval: 0.5.
a: Inverse pole figure for the inferred shear plane normal.
b: Inverse pole figure for the inferred shearing direction.

about the macroscopic fabric axes; and (3) An almost identical character in the preferred orientation of positive and negative forms, giving a hexagonal character to the fabric (see figure 4 in Schmid et al, 1981b). Thus, the character of the preferred orientation can be approximated by two trigonal quartz crystals with their c-axes parallel to the Y-direction, one in a positive and one in a negative orientation.

Bunge and Wenk [1977] found an identical fabric in their specimen Sci 293, collected in the Gruf complex (Pennine nappes of Switzerland), which deformed under amphibolite facies conditions. Wilson [1975] measured optical pole figures of this type in a mylonite from the Swedish Caledonides, deformed under at least upper greenschist facies conditions. It seems that fabrics of this type are common in higher grade metamorphic terrains.

There is a smooth transition from this type of fabric into single girdles of the type represented by specimen P 248. The a-axis pole figures of the specimens Gran 133 and P 248 are almost identical.

Recently, Bouchez et al. [1984] reinterpreted a fabric characterized by a single c-axis maximum parallel to the lineation defined by elongate quartz grains (specimen GAE 9, Schmid et al., 1981b) to be a fabric of the type described above. They argue that the quartz grains define a false lineation and that the real stretching lineation is parallel to what Schmid et al [1981b] considered to be the intermediate strain axis Y. We do not, as yet, regard their reinterpretation, based on a particular model for the reorientation of rutile needles, to be conclusive. Until this question is definitely resolved we would not like to propose a separate class of c-axis fabrics based on this single specimen. It has to be emphazised, however, that Bouchez et al. [1984] overlooked the fact that the fabric of GAE 9 is not identical to that found in specimens Gran 133 and Sci 293 even if the principal strain axes X and Y are exchanged: specimen GAE 9 has a very strong trigonal character, whereas the two other specimens have an almost perfect hexagonal character.

3. Crossed C-axis Girdles.

Sander [1970] proposed a division of c-axis crossed girdles into pseudo-two-girdle and two-girdle patterns and Lister [1977] subsequently renamed them type I and type II crossed-girdle fabrics, respectively. The type I crossed girdles are far more common and they are characterized by the tendency of two c-axis girdles to meet at some distance from the intermediate strain axis Y and to be connected through Y via a single girdle more or less orthogonal to the foliation plane (see specimen PT 463 in figure 5). Consequently the c-axes only approximately populate two intersecting great circles. The type II crossed girdles are less common and they are characterized by two girdles meeting at a point parallel to the intermediate strain axis Y (SE 85 in figure 5).

Type I crossed girdles. Specimen PT 463 exhibits a type I crossed girdle, and the main features of its fabric are illustrated in figure 10. A series of favoured crystal orientations along the skeletal outline of the c-axis pole figure (figure 10a) were selected and plotted in figure 10b,c,d.

The favoured orientations of crystals whose c-axes lie near the Y-axis (positions 4-10) is such that two of the three a-axes always align with a direction near the margin of the pole figure, 30° away from the lineation (see also the a-axis maxima in figure 5). These positions have a common normal to the first order prisms m located parallel to the lineation. Figure 10c also contains information on the favoured positions of the negative rhombs z, but it can be seen from figure 10 that positive and negative rhombs are exchangeable in the case of position 7 (along a trace parallel to PSI 2 at PHI = 0° two maxima are found, 60° apart in PSI 2). As one moves away from the intermediate strain axis to position 4, the maximum at PSI 2 > 60° becomes stronger (figure 10e). An analogous observation can be made in moving towards position 10, except that now the maximum at PSI 2 < 60° is stronger (right half of the diagram in figure 10e at PHI > 90°). Thus, the character of the fabric goes from hexagonal at position 7 towards a more trigonal character at positions 4 and 10. The preferred orientation of the negative forms at positions 4, 5, 9, and 10 follows the trend of one of the two girdles outlined in figure 10 and described below.

As the c-axis positions move away from the Y-axis the crystals must align their <a>direction with one or the other of the two a-axis maxima illustrated in figure 5. This causes a splitting of the single girdle around the Y direction into the two crossed girdles. Positions 1-5 and 9-13 (figure 10b) show the alignment of one of the <a> directions at 30° from the lineation and the alignment of the poles to the negative rhombs at a position 90° away from the a-axis maximum and near the margin of the pole figure (note that the <a> and <z> directions are orthogonal). Figure 10d covers the other of the two girdles and it is seen that the favoured crystal orientations in this figure are just the mirror image of those plotted in figure 10b.

The favoured crystal orientations for grains with their c-axes at the margin of the pole figure is best discussed using figure 10f, which is a section through the ODF at PHI = 90°. Two elongate maxima are aligned parallel to the PSI 2 axis at two positions in PSI 1. They correspond to the two girdles at the margin of the pole figure. The degree of preferred orientation of crystal directions other than the c-axis is very weak and no significant maxima

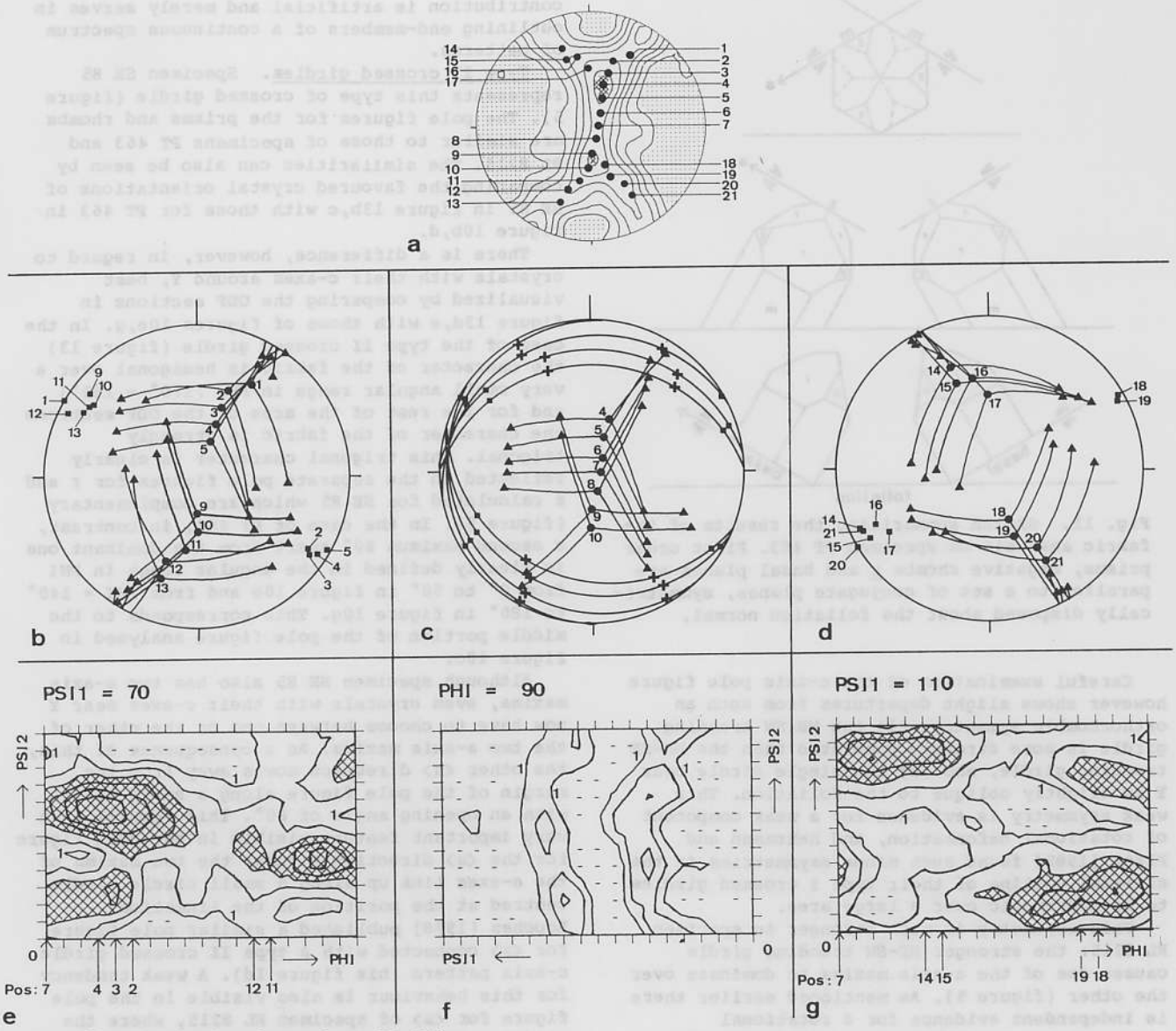

Fig. 10. Analysis of specimen PT 463.
a: c-axis pole figure; contour interval: 0.5.
b,c,d: Favoured crystal orientations for the selected c-axis positions numbered in figure 10a. Dots: c-axis positions; triangles: poles to the negative rhombs z; squares: a-directions; crosses: poles to the first order prisms.
e,f,g: Selected sections through the ODF. Order of expansion: 10; contour interval: 1.0.

appear at particular values of PSI 2 as is the case in figures 10e and 10g.

Figure 11 summarizes the main features of this complicated fabric in the form of a sketch which displays the favoured crystal orientations. Two first order prisms m, two negative rhombs z, or two basal planes favour an orientation parallel to two planes symmetrically disposed about the foliation and at an angle of 60° away from the foliation normal.

The type of fabric found along one of the two girdles is very similar to that found in the case of the single girdle fabric of specimen R 405. This can be seen easily by comparing figures 10b and 7b or figures 10e and 7c. Because the second girdle described by figure 10d is the mirror image of that described by figure 10b we can think of the crossed girdle fabric as being a combination of two single girdle patterns, one being the mirror image of the other. This leads to an overall orthorhombic symmetry in the fabric.

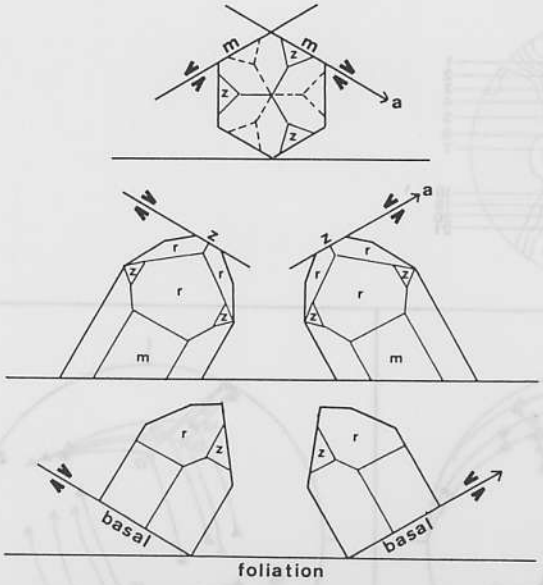

Fig. 11. Sketch summarizing the results of the fabric analysis on specimen PT 463. First order prisms, negative rhombs z and basal planes are parallel to a set of conjugate planes, symmetrically disposed about the foliation normal.

Careful examination of the c-axis pole figure however shows slight departures from such an orthorhombic symmetry: (1) the NE-SW trending girdle is more strongly populated than the NW-SE trending girdle, and (2) the single girdle near Y is slightly oblique to the foliation. This weak asymmetry is evidence for a weak component of rotational deformation, and Behrmann and Platt [1982] found such minor asymmetries in the skeletal outline of their type I crossed girdles to be systematic over a large area.

This asymmetry is much stronger in specimen RL 8215: the stronger NE-SW trending girdle causes one of the a-axis maxima to dominate over the other (figure 5). As mentioned earlier there is independent evidence for a rotational component in the deformation of this specimen from microstructural criteria. The inspection of figures 12b and 12c shows that the main character of the fabric is unchanged except for the unequal strengths of the two girdles.

Measurements on other specimens not included in figures 4 and 5 indicate that there is a smooth transition from near orthorhombic crossed girdles through asymmetric crossed girdles to single girdles of the type of CC 1. Note that the c-axis girdle of CC 1 has a kinked skeletal outline: the c-axes only approximately lie on a great circle. Lister and Williams [1979] extended the term type I crossed girdle to include fabrics of the kind of specimen CC 1, but here we grouped CC 1 into a separate class. In view of the transitions observed it is important to realise that the classification made in this contribution is artificial and merely serves in outlining end-members of a continuous spectrum of patterns.

Type II crossed girdles. Specimen SE 85 represents this type of crossed girdle (figure 5). The pole figures for the prisms and rhombs are similar to those of specimens PT 463 and RL 8215. The similarities can also be seen by comparing the favoured crystal orientations of SE 85 in figure 13b,c with those for PT 463 in figure 10b,d.

There is a difference, however, in regard to crystals with their c-axes around Y, best visualized by comparing the ODF sections in figure 13d,e with those of figures 10e,g. In the case of the type II crossed girdle (figure 13) the character of the fabric is hexagonal over a very small angular range in PHI (170° - 180°) and for the rest of the area of the ODF sections the character of the fabric is strongly trigonal. This trigonal character is clearly reflected in the separate pole figures for r and z calculated for SE 85 which are complementary (figure 5). In the case of PT 463, in contrast, a second maximum 60° apart from the dominant one is clearly defined in the angular range in PHI from 0° to 50° in figure 10e and from PHI = 140° to 180° in figure 10g. This corresponds to the middle portion of the pole figure analysed in figure 10c.

Although specimen SE 85 also has two a-axis maxima, even crystals with their c-axes near Y now have to choose between one or the other of the two a-axis maxima. As a consequence of this, the other <a> direction moves away from the margin of the pole figure along a small circle with an opening angle of 60°. This results in a very important feature visible in the pole figure for the <a> direction figure: the two maxima of the a-axes link up along a small circle girdle centred at the position of the lineation. Bouchez [1978] published a similar pole figure for <a> connected with a type II crossed girdle c-axis pattern (his figure 1d). A weak tendency for this behaviour is also visible in the pole figure for <a> of specimen RL 8215, where the middle segment of the c-axis crossed girdle is not as strongly developed as in PT 463.

Optical data on type II crossed girdles have been described by Sander [1970], Sylvester and Christie [1968] and Bouchez [1977]. Sander [1970] found them in "rodded B-tectonites" (page 592-593) and Bouchez [1977] carried out strain estimates based on aspect ratios of porphyroclasts and found k-values between 1.15 and 8.15. Thus, there is strong evidence that type II crossed girdles (at least those with a small opening angle between the two girdles) are typical for constrictional strain.

4. Small Circle C-axis Girdles.

In this type of pattern, the c-axes form maximum concentrations along a small circle cent-

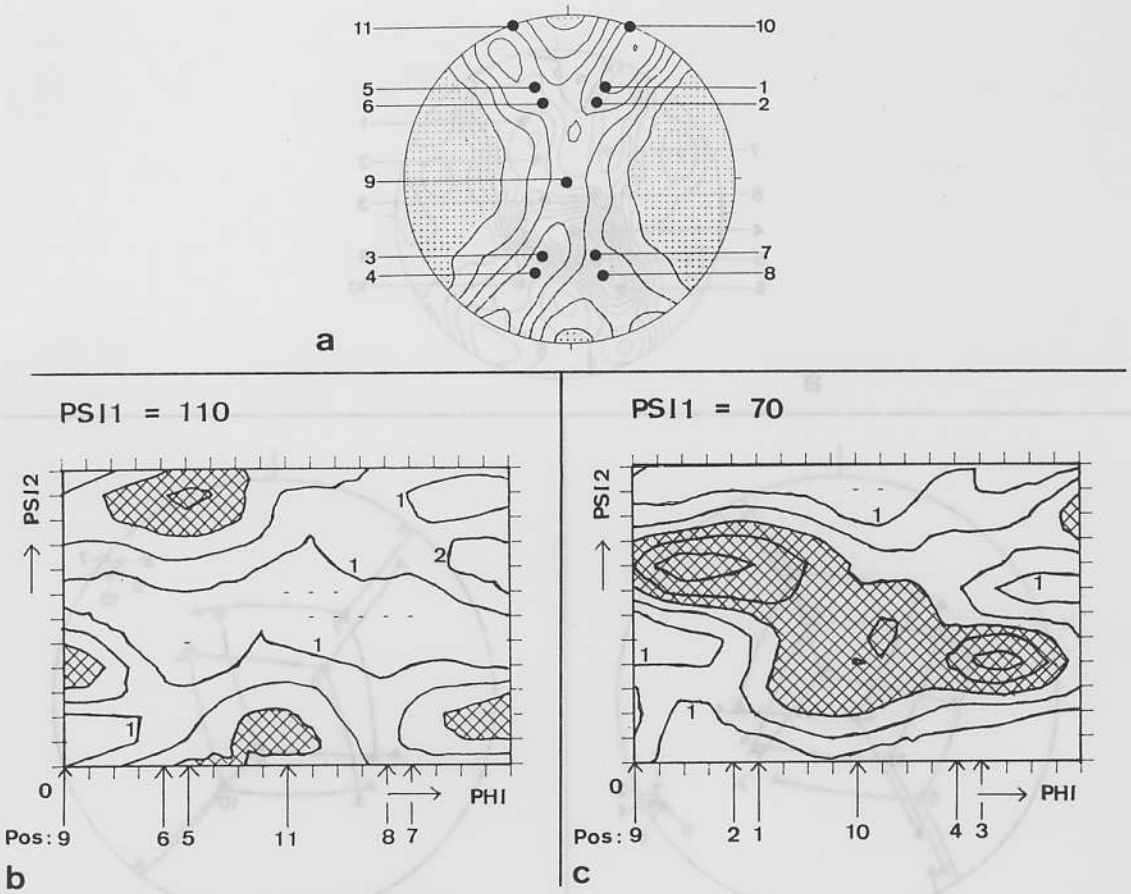

Fig. 12. Analysis of specimen RL 8215.
a: c-axis pole figure, contour interval: 0.5.
b,c: Selected sections through the ODF. Order of expansion: 10; contour interval: 1.0.

ered around the pole to the foliation. It is of special interest because it is directly comparable with the quartz fabrics found in experimental rock deformation [Tullis et al, 1973]. Gran 125 exhibits such a pattern and RL 8330 is of a transitional character towards type I crossed girdles.

As expected from the distribution of the c-axes along a small circle with opening angles of 25° (RL 8330) and 40° (Gran 125), the a-axes have to spread along a small circle with a high opening angle and this is seen in the pole figures for <a> (figure 5). RL 8330 shows its transitional character in the a-axis pole figure as well: two relatively weak maxima form at the margin of the pole figure.

The character of the pole figures for r and z of specimen RL 8330 is very surprising (the same pole figures for Gran 125 are low quality). What appeared to be a fabric of orthorhombic symmetry with respect to to the c-axes and the prisms turns out to be of a lower symmetry with respect to the rhombs. The favoured crystal orientations for crystals aligned with their c-axes parallel to the two maxima in the c-axis pole figure have a strong preference to position one of their positive rhombs so as to coincide with the strong point maximum visible in the r pole figure, while the a-axes are positioned at 30° away from the margin of the pole figure. The c-axes at the margin of the pole figure are non-selective in regard to other crystal directions as was observed for PT 463 (figure 10f).

The inverse pole figures for the foliation normal are very similar to those obtained by Tullis et al. [1973] in their high temperature experiments and almost identical to those calculated by Riekels and Baker [1977] for a fabric similar to that of RL 8330: the positive forms are preferred over the negative ones for the normal to the foliation or the shortening direction, respectively. Both the opening angle of the c-axis girdle and the distance of the maximum in the inverse pole figure from the c-axis is larger for Gran 125 which was deformed at higher temperatures than RL 8330. This agrees well with the trend found in the experiments of Tullis et al. [1977].

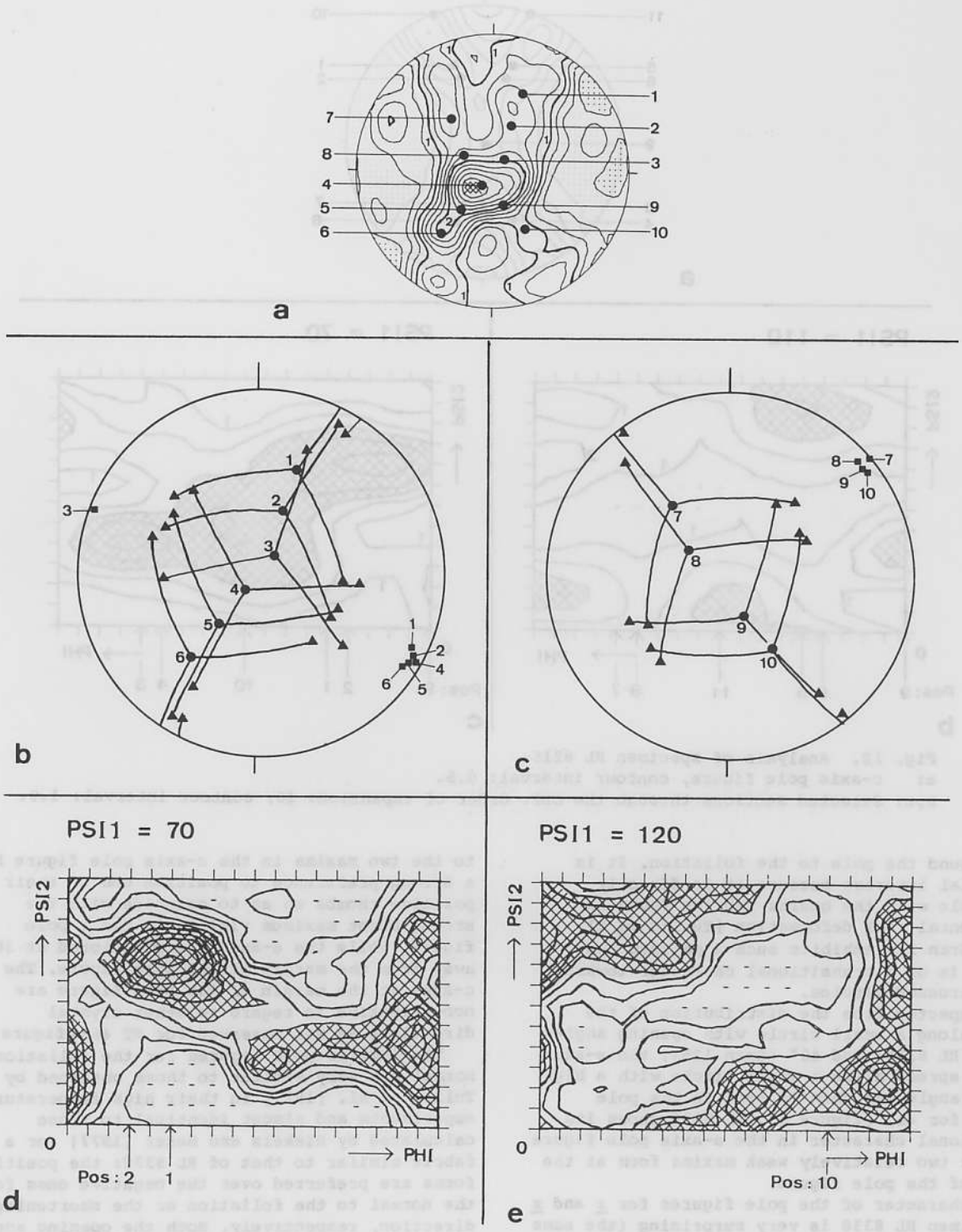

Fig. 13. Analysis of specimen SE 85.
a: c-axis pole figure, contour interval 0.25.
b,c: Favoured crystal orientations. Dots: c-axes; triangles: poles to negative rhombs; sqaures: a-axes.
d,e: Selected sections through the ODF. Order of expansion: 10; contour interval: 0.5.

The similarities of the fabric found in specimen RL 8330 and that analysed by Riekels and Baker [1977] are striking. These authors carried out a complete fabric analysis on a mylonite collected in the same locality along the Moine Trust, and they were the first to emphasize the similarities with the fabrics of Tullis et al. [1973]. Law et al. [1984] studied c-axis fabrics along the northernmost portion of the Moine Thrust and they found small circle girdles, type I crossed girdles and patterns transitional between those two end-members. Their strain analysis on detrital grains shows that the small circle girdles correlate with k-values less than 1 (flattening) and that type II crossed girdles correlate with approximately plane strain. A similar correlation was also found by Marjoribanks [1974].

Interpretation of the Analyzed Fabrics

1. The Dominating Role of Slip in the Crystallographic <a> Direction.

From the character of the single c-axis girdle fabrics described in an earlier section it is obvious that the pole figures for the <a> direction play a key role in the interpretation of quartz fabrics, a fact emphasized by Bouchez [1978]. There is much evidence for slip in the direction of <a> from experiments on quartz single crystals. <a> slip was found to operate in the basal plane (0001), the steep rhombs $\{10\bar{1}2\}$ and $\{01\bar{1}2\}$, the positive and negative rhombs $\{10\bar{1}1\}$ and $\{01\bar{1}1\}$, and first order prisms $\{10\bar{1}0\}$ [for references see Carter, 1976, and a recent compilation of reported slip systems in Linker et al., 1984]. It is important to note that the rhombohedral planes contain one possible <a> slip direction only, whereas the basal plane contains three <a> directions. Slip on the first order prisms forms another special case because it allows simultaneous slip on two $\{10\bar{1}0\}$ forms in two different <a> directions, producing plane strain deformation orthogonal to the c-axis.

The other possible slip directions reported in the literature are <c> and <c+a>. Linker et al. [1984] found that the <a> direction is very much easier to operate than the <c+a> direction. On the other hand slip in the <c> direction produced the fastest strain rates in their experiments. The only evidence based on a fabric analysis for the occurrence of <c> slip in naturally deformed quartz comes from specimen GAE 9 [Schmid et al., 1981b]. The perfect trigonal character of this fabric may be the result of slip in the <c> direction being dependent on the sign of the resolved shear stress. This would be expected for alpha quartz by virtue of symmetry considerations [Groves and Kelly, 1963]. Therefore, the trigonal character of this fabric could well have resulted from rotational deformation under conditions favouring <c> slip.

2. Single Girdle Patterns as Indicators of Active Slip Planes.

The data from specimens CC 1 and R 405 strongly support the interpretation of the single girdle c-axis pattern as resulting from simple shear deformation as proposed by Burg and Laurent [1978], Bouchez et al. [1979] and many other workers. This conclusion is supported by the findings of Etchecopar [1977]: the single girdle patterns are the result of the preferred alignment of a-axes into parallelism with the bulk shearing direction in the rock and the preferred alignment of the active slip planes with the bulk shear plane. This makes the single girdles particularly interesting for inferring the relative importance of the various slip systems by correlating the tendency of a particular crystallographic plane to align with the shear plane in the bulk rock with the relative slip activity along these crystallographic planes.

The inverse pole figures for the inferred shear plane normal presented in figures 6, 7, 8, and 9 indicate different amounts of activity on the basal plane, the rhombs, and the first order prisms for the four specimens. CC 1 and R 405 are interpreted to have been deformed primarily by slip on the rhombs, with minor activity of the basal plane and the prisms m. C 156 deformed predominantly by basal slip. In P 248 there is no activity on the basal plane and prism slip is more important. This latter specimen deformed under higher temperatures compared to the other three specimens and this agrees well with the transition towards prism slip with increasing temperatures, as found in the experiments of Tullis et al. [1973]

The activity on positive and negative forms was unequal in the case of CC 1 and R 405. Stress induced Dauphiné twinning has been shown to produce a strong selectivity with regard to positive and negative forms [Tullis and Tullis, 1972]. This mechanism can be ruled out to be a major influence on the preferred orientation of r and z in our specimens on the basis of the character of the separate pole figures for r and z (figure 4): the r pole figure of specimen CC 1 is strikingly similar to the z pole figure of specimen R 405 although the orientation of the principal stress directions must have been the same for both specimens (dextral simple shear).

None of the inverse pole figures for the movement direction (figures 5d, 6d, 7 and 8) indicates a second maximum at <c+a> or <c>. From this we conclude that to a first approximation <a> is the only operative slip direction.

3. Single Girdles as Indicators of Shearing Deformation.

In the case of specimens CC 1 and R 405 there is independent evidence that the deformation path closely approximates conditions of simple shearing. Specimens C 156 and P 248 provide

microstructural evidence for at least a strong component of rotational deformation.

The asymmetry of single girdle fabrics has been extensively used as an indicator for the sense of shearing [Simpson and Schmid, 1983]. Care has to be taken during sample collection in order to ensure that the deformation within the specimen analyzed is representative of the deformation of the entire volume of the rock under consideration [Lister and Williams, 1979]. Garcia Celma [1983] demonstrated that the sense of movement around rigid lenses may even be opposite to that of the bulk shear zone.

The single girdle fabrics measured for the four specimens mentioned above agree with the predictions of Etchecopar [1977] for the simple shearing deformation, based on a two dimensional model which considers one slip direction only. This agreement is due to the fortunate circumstance that one unique slip direction in <a> is operative in these specimens.

If the intracrystalline slip activity is restricted to one single <a> direction aligning with the bulk shearing direction during progressive simple shear, the amount of shear strain may ideally be determined from measuring the angle between the dominant a-axis maximum and the lineation in the rock. The measurements made in the case of specimens CC 1 and R 405 are indeed compatible with this simple inference.

Unfortunately, the situation is more complicated in most cases for several reasons: (1) the macroscopically visible lineation and foliation need not be exactly parallel to the principal axes of finite strain, (2) strain partitioning between different domains within a simple shear zone may lead to complications [Lister and Williams, 1980, 1983], (3) during the initial stages of simple shearing a strong fabric in terms of a perfect alignment of <a> directions with the bulk shearing direction is not yet established, and (4) even at large strains <a> slip may not be restricted to a direction parallel to the bulk shearing direction.

In many mylonite zones the angle between the dominant a-axis maximum and the lineation is too large to account for the large shear strains expected from independent evidence [Boullier and Quenardel, 1981]. In such cases, however, the c-axis pole figure exhibits a transitional character between a single c-axis girdle and a type I crossed girdle . Whether this is due to a departure from ideal simple shearing conditions or to the simultaneous operation of <a> slip in an antithetic sense to the overall shear sense during simple shearing is not clear.

Figure 14 sketches the transition from type I crossed girdles into single c-axis girdles. This transition may represent an increasing rotational component in the strain path. Alternatively, a similar trend is expected with increasing strain during simple shearing as suggested by the work of Garcia Celma [1983] on naturally deformed quartzites and by the simple shear experiments on ice carried out by Bouchez and Duval [1982].

4. Type I Crossed Girdles as Indicators of Coaxial Deformation under Plane Strain.

An interpretation of type I crossed girdles with a high degree of orthorhombic symmetry (PT 463) can be based on symmetry arguments [Paterson and Weiss, 1961] and on the summary of the favoured crystal orientations given in figure 11. To a first approximation the lattice preferred orientation exhibits an orthorhombic symmetry related to the finite strain axes (homotactic fabric, Sander, 1970) and this implies a coaxial strain path such as was found in the numerical simulations of pure shear by the model work of Etchecopar [1977] and Lister and Hobbs [1980].

Figure 11 suggests the alignment of first order prisms, negative rhombs and basal planes in a set of planes symmetrically disposed about the foliation normal and parallel to the intermediate strain axis Y. If the <a> direction is again inferred to be the only important operating slip direction, analogous to the inferences made for the interpretation of single c-axis girdle fabrics, conditions of plane strain can be deduced from the alignment of the a-axis maxima with the X-Z section of the finite strain ellipsoid. We postulate slip in the <a> direction to also dominate in the case of the type I crossed girdles on the basis of: (1) the striking similarities in terms of favoured crystal orientations found along one of the two girdles in PT 463 with those found along the single girdle of specimen R 405, and (2) the smooth transitions from ideal c-axis girdles (R 405) via c-axis girdles with a kinked skeletal outline (CC 1) and asymmetric crossed girdles (RL 8215) into near-symmetric crossed girdles (PT 463).

At this point it may be useful to reconsider some details in the ODF of PT 463 described earlier and supporting our interpretation of type I crossed girdles. It was found (figure 10f) that crystals with their c-axis at the periphery of the pole figure are not very selective in positioning their other crystal directions into favoured orientations. This can be elegantly explained in terms of our postulate that basal slip operates preferentially in the case of such crystals. Basal slip does not require a particular <a> direction to align with the X-Z section of the strain ellipsoid because plane strain deformation can be achieved by a shared activity along two of the <a> directions within the basal plane. The interpretation that slip on the negative rhombs predominates in crystals with their c-axis at some distance from the Y direction is supported by the trigonal character of the ODF for such c-axis positions. For

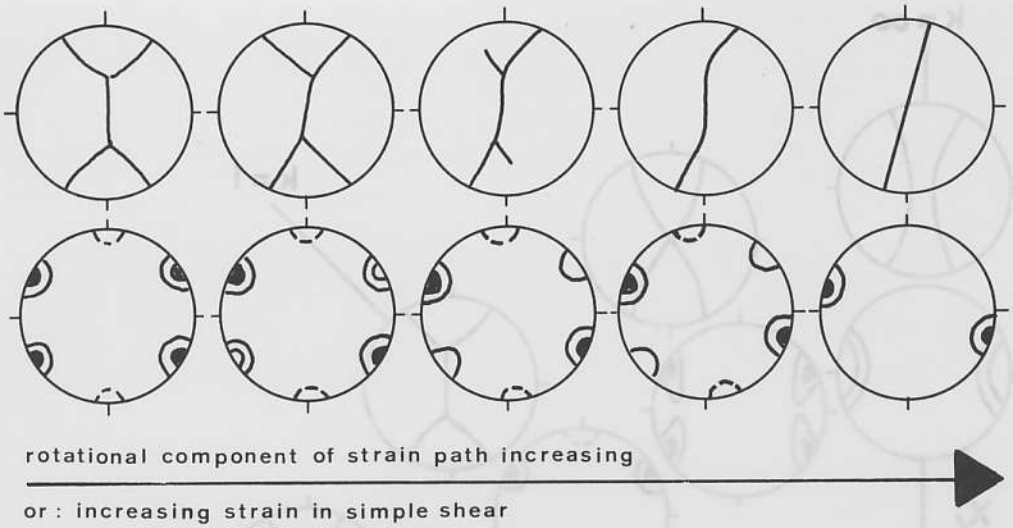

Fig. 14. Sketch of the main features of the pole figures for the c-axis and the a-axes expected for rotational deformation with a dextral sense of movement. The c-axis pole figures are sketched in the form of a skeletal outline. The pole figures for the a-direction are sketched in the form of schematic contour intervals.

crystals with their c-axis aligned with the Y direction a hexagonal character was found in the ODF, consistent with the idea of prismatic slip for this group of crystals.

Crystals with their c-axis parallel to the Y direction are in a special situation with regard to coaxial plane strain deformation: conjugate shear can simultaneously operate on two first order prisms within the same crystal. In the case of crystals with their c-axis away from Y, i.e. crystals deforming by slip on the rhombs and the basal plane, the shearing deformation on the scale of the grains has to deviate from the imposed overall deformation of the grain aggregate which is coaxial if <a> is the only operative slip direction. This follows from the van Mises requirement for five independent slip systems [Paterson, 1969], if a polycrystalline aggregate is to undergo homogeneous deformation on the scale of individual grains. The results of elaborate work in terms of an "axial distribution analysis" (A.V.A. of Sander, 1970) seem to suggest a systematic spatial distribution of grains oriented for slip along one or other of the two conjugate shear planes, represented by the crossed girdles.

It was mentioned earlier that PT 463 exhibits a slight departure from an ideal orthorhombic symmetry. This departure is more pronounced in RL 8215 and we interpret this to indicate a strain intermediate between that of simple shear and coaxial strain under plane strain conditions. Asymmetric type I crossed girdles are widespread in many mylonite zones (Moine Thrust, Law et al., 1984; Simplon Fault, Mancktelow, in press; Insubric Line, unpublished results) and this suggests a more complex strain path than that of simple shear. It seems that ideal simple shear is exceedingly rare in mylonite belts.

The interpretation of fabrics with a c-axis point maximum parallel to Y (Gran 133) in terms of plane strain deformation associated with a high activity of prism slip now becomes obvious. It is likely that this deformation involves a rotational component in the case of Gran 133, because the a-axis maxima are asymmetrically disposed with regard to the finite strain axes. No kinematic inference can be made on the basis of the c-axis pole figure alone.

5. Type II Crosed Girdles and Small Circle C-axis Girdles as Indicators of Departures from Plane Strain.

Departures from conditions of plane strain are indicated in the interpretation of the a-pole figures in the case of specimens SE 85, RL 8330, and Gran 125 (to a smaller extent also in RL 8215). In the case of the type II crossed girdle fabric of SE 85 the a-axis maxima are connected via a small circle around the lineation. This implies a component of cylindrical flow in the constrictive domain, as already postulated by Bouchez [1978], who additionally carried out strain measurements on porphyroclasts. Duplex slip on the first order prisms is not suitable for producing constrictional strain and consequently slip on the negative rhombs predominates in the case of the type II crossed girdles (strongly trigonal character of the ODF). The c-axis pattern of type II crossed girdles is a direct consequence of: (1) the alignment of the a-axes, and (2) the minor role of prism slip which was responsible for the connecting single girdle near Y in the

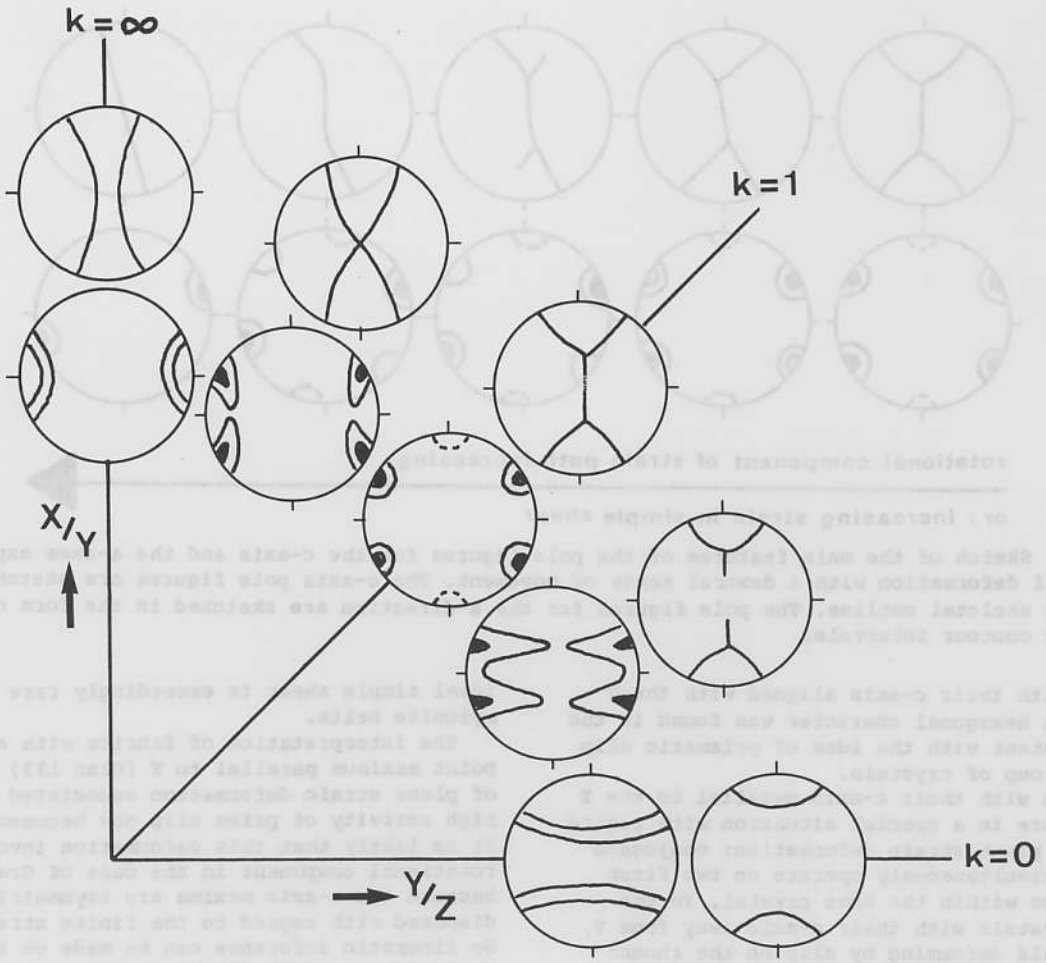

Fig. 15. Sketch of the main features of the pole figures for the c-axis and the a-axes expected for coaxial deformation within different areas of the Flinn diagram. k=1 corresponds to plane strain, k>1 implies constriction, k<1 implies flattening.

case of the type I crossed girdles (figure 10c). The comparison between type I and type II crossed girdles suggests that the activity of particular slip systems is not exclusively dictated by factors such as temperature and strain rate, but also by the type of strain imposed on the aggregate.

In specimens RL 8330 and Gran 125 the a-axis maxima have a tendency to spread along high angle small circles centred around the foliation normal and this suggests flattening strains. This interpretation is on a very firm basis in view of the strain estimates carried out on porphyroclasts (specimen RL 8330 and measurements carried out by Law et al., in press), and also in view of the similar patterns obtained in experimental rock deformation of quartzites [Tullis et al., 1973]. The c-axis pole figure of specimen RL 8330 is transitional between the type I crossed girdle and the small circle c-axis pattern and consequently suggests a deformation intermediate between that of flattening and plane strain. The asymmetry detected in the pole figures for the rhombs suggests a rotational component of strain in specimen RL 8330.

The types of pole figures for the directions of <c> and <a> expected during coaxial deformation within different fields of a Flinn diagram are summarized in figure 15.

Summary and Discussion of the Mechanisms of Lattice Reorientation.

The principal features of our empirical interpretation based on a complete fabric analysis can be summarized as follows: (1) the alignment of a-axis maxima with the shearing direction during simple shear led us to conclude that the <a> direction is the only significant slip direction and it was shown that the resulting fabric can be interpreted in terms of

crystal orientations favoured for easy slip; (2) The concept of easy slip was extended for the case of coaxial deformation in plane strain, which in our interpretation results in favoured crystal orientations for easy slip along two conjugate planes, whose orientation is crystallographically controlled; (3) The interpretation of fabrics developed in the flattening and constriction fields is essentially based on the features seen in the pole figures for the <a> direction which was implicity assumed to be the only significant slip direction; (4) In our interpretation the degree of preferred orientation of a particular intracrystalline slip plane into favoured crystal orientations was equated with the amount of activity on these particular slip planes.

Generally, the type of lattice preferred orientation found in quartzites is largely independent of the amount of syntectonic recrystallization and the interpretation of the fabrics demonstrated that they are controlled by the active slip systems, the type of finite strain, and the kinematic framework. The fabrics described in this contribution are primarily caused by intracrystalline plasticity (low temperature plasticity or power law creep) and we have to look for a slip induced mechanism of lattice reorientation. A mechanism of lattice reorientation based on recrystallization driven by differences in the elastic strain energy within individual grains [Kamb, 1959, 1961] is therefore unrealistic. Nevertheless, syntectonic recrystallization has a profound effect on the mechanism of lattice reorientation. We first confront our fabric interpretation with numerical models for slip induced lattice reorientation, and then we will discuss this important role of syntectonic recrystallization during lattice reorientation.

Two numerical models based on slip induced lattice reorientation have been proposed: the model of Etchecopar [1977] and the model of Lister et al. [1978]. Etchecopar [1977] invokes local bulk rotations of grains, caused by heterogeneous deformation on the scale of individual grains. In the model of Lister et al. [1978] the lattice reorientation is caused by vorticity imbalance during homogeneous deformation of a grain aggregate deforming by multiple slip. Lister [1982] pointed out very clearly that these two models for slip induced lattice reorientation are fundamentally different and that future work needs to take both models into account.

Our fabric interpretation leads us to believe that heterogeneous deformation on the scale of individual grains is very important. This is one of the reasons why the model of Etchecopar [1977] offers a satisfactory prediction, whereas the Lister model [Lister and Hobbs, 1980] fails to predict single c-axis girdles. In coaxial deformation the prediction of Lister and Hobbs [1980] yields a close resemblance to the patterns summarized in figure 14. Yet our interpretation of the type I crossed girdles is incompatible with homogeneous deformation. This indicates that both mechanisms of slip-induced lattice reorientation must be operative: a mechanism taking account of heterogeneous deformation associated with local bulk rotations of grains (the model of Etchecopar) and a mechanism involving the lattice reorientation caused by the vorticity imbalance during homogeneous deformation (the model of Lister et al.).

One important feature of many quartz fabrics is the strong tendency for individual grains to align <a> directions into one maximum (simple shear) or into maxima which are 60° apart (pure shear) and which are crystallographically controlled. This feature cannot be directly confronted with the results of the models mentioned. Etchecopar [1977] used a two dimensional approach, and Lister and Hobbs [1980] primarily discuss c-axis patterns, and information on other crystal directions is not available apart from a few pole figures for the <a> direction predicted for simple shear (their figure 15). In these a-pole figures only a weak preferred alignment of <a> directions with the shear direction can be observed. The observed high degree of alignment of <a> directions suggests that the relative activity of the various slip planes varies from grain to grain while the <a> slip direction remains in a constant orientation from grain to grain. It would be an interesting task for future TEM work to look for possible dislocation interactions between neighbouring grains.

A serious shortcoming of the model of Etchecopar [1977] is that it is physically unrealistic. It is interesting to note, however, that a strong tendency for the dominant slip plane to align with the shear plane during simple shear results mainly from the pull-apart of "locked" grains which is built into this model. The locked grains in this model are those grains which help to maintain a two maximum pattern (or a crossed girdle pattern in three dimensions) up to shear strains as high as $\gamma = 2$. The single maximum (or single girdle pattern in three dimensions) develops by the passive local bulk rotation of the pull-apart fragments into the orientations for easy slip.

By now taking into account the influence of syntectonic recrystallization we propose a physically different model which can lead to the same end result as the model of Etchecopar [1977]. The grains in a locked position are those which have a very low resolved shear stress on crystallographic planes of easy slip. Consequently, these grains deform less than the surrounding aggregate and they have to use alternative slip systems which are harder to activate. Since those locked grains are local stress raisers their dislocation density will be higher than that of the surrounding grains. Thus, they will be preferentially affected by

syntectonic recrystallization driven by the build-up of distortional lattice energy. The subgrain rotation mechanism will create new grains with a different lattice orientation more favourable for easy slip, whereas the grain boundary migration mechanism will lead to the preferential consumption of grains with a high distortional lattice energy. Instead of the rotation of pull-apart fragments of locked grains, as in the Etchecopar [1977] model, it is the preferential syntectonic recrystallization of locked grains which will lead to an end orientation for easy slip. We thus propose that syntectonic recrystallization promotes stable end-orientations for which the imposed deformation causes the minimum dissipation of energy by the active slip systems. Bouchez and Duval [1982] interpreted their fabric produced in simple shear of ice in a very similar way.

Since irrotational deformation leads to a fabric in terms of easy slip along two conjugate shear planes we propose that dynamic recrystallization and heterogeneous deformation play a similar role in lattice reorientation as in the case of shearing deformation. This, together with the interpretation that <c+a> slip is unimportant, is primarily responsible for the minor discrepancies in the c-axis pole figures and the substantial differences in the pole figures for <a> when the analysed fabrics are compared with the predictions of Lister and Hobbs [1980].

It is hoped that our understanding of fabric development will advance from future work on modelling, taking account of more than one mechanism of slip induced lattice reorientation, together with experiments under conditions other than those of coaxial flattening and TEM work directed towards a better understanding of dislocation interactions between neighbouring grains.

Acknowledgements. We are grateful for the cooperation of the following colleagues who not only provided us with specimens but also helped in establishing the geological framework in which these specimens were deformed: Jan Behrmann, Inge Frey, Amparo Garcia Celma, Richard Law, Daniel Müller, Carol Simpson, John Starkey and Andre Zingg. We also profited from discussions with Jean-Luc Bouchez, Rob Knipe, Gordon Lister, Neil Mancktelow and Jan Tullis. Gordon Lister, Neil Mancktelow, Jan Tullis, Molly Welker and an anonymous reviewer helped to improve the first version of the manuscript. M. Casey acknowledges financial support from the Swiss Nationalfonds project no. 2.080-0.83. Ernie Perkins and Sven Girsberger are thanked for provision of advice and microcomputer facilities for the production of the typescript.

References

Baker, D. W., H. R. Wenk, and J. M. Christie, X-ray analysis of preferred orientation in fine-grained quartz aggregates, J. of Geology, 77, 144-172, 1969.

Baker, D. W., and H. R. Wenk, Preferred orientation in a low-symmetry mylonite, J. of Geology, 80, 81-105, 1972.

Behr, H. J., Beiträge zur petrographischen und tektonischen Analyse des sächsischen Granulitgebirges, Freib. Forschungsh., Reihe C, 119, 1-146, 1961.

Behr, H. J., Zur Methodik tektonischer Forschung im kristallinen Grundgebirge, Ber. Geol. Ges. DDR., 10, 163-179, 1965.

Behrmann, J. H., and J. P. Platt, Sense of nappe emplacement from quartz c-axis fabrics; an example from the Betic Cordilleras (Spain), Earth and Planet. Sci. Letters, 59, 208-215, 1982.

Bouchez, J. L., Plastic deformation of quartzites at low temperature in an area of natural strain gradient, Tectonophysics, 39, 25-50, 1977.

Bouchez, J. L., Preferred orientations of quartz a axes in some tectonites: kinematic inferences, Tectonophysics, 49, T25-T30, 1978.

Bouchez, J. L., and P. Duval, The fabric of polycrystalline ice deformed in simple shear: Experiments in torsion, natural deformation and geometrical interpretation, Textures and Microstructures, 5, 171-190, 1982.

Bouchez, J. L., and A. Pecher, The Himalayan Main Central Thrust Pile and its quartz-rich tectonites in Central Nepal, Tectonophysics, 78, 23-50, 1981.

Bouchez, J. L., P. Dervin, J. P. Mardon, and M. Englander, La diffraction neutronique appliquée à l'étude de l'orientation préférentielle de réseau dans les quartzites, Bull. Minéral., 102, 225-231, 1979.

Bouchez, J. L., D. H. Mainprice, L. Trepied, and J. C. Doukhan, Secondary lineation in a high-T quartzite (Galicia, Spain): an explanantion for an abnormal fabric, J. Structural Geology, 6, 159-165, 1984.

Boullier, A. M., and J. M. Quenardel, The Caledonides of northern Norway: relation between preferred orientation of quartz lattice, strain and translation of the nappes, in: Thrust and Nappe Tectonics, edited by K. R. McClay and N. J. Price, Geol. Soc. Spec. Public., 9, 185-195, 1981.

Bunge, H. J., Mathematische Methoden der Texturanalyse, 330 pp., Akademie-Verlag, Berlin, 1969.

Bunge, H. J., and H. R. Wenk, Three-dimensional texture analysis of three quartzites (trigonal crystal and triclinic specimen symmetry), Tectonophysics, 40, 257-285, 1977.

Burg, J. P., and P. Laurent, Strain analysis of a shear zone in a granodiorite, Tectonophysics, 47, 15-42, 1978.

Carreras, J., A. Estrada, and S. H. White, The effects of folding on the c-axis fabrics of a quartz mylonite, Tectonophysics, 39, 3-24, 1977.

Carter, N. L., Steady state flow of rocks, Rev. Geoph. Space Phys., 14, 301-360, 1976.

Casey, M., Numerical analysis of X-ray texture data: An implementation in FORTRAN allowing triclinic or axial specimen symmetry and most crystal symmetries, Tectonophysics, 78, 51-64, 1981.

Eisbacher, G. H., Deformation mechanics of mylonitic rocks and fractured granites in Cobequid Mountains, Nova Scotia, Canada, Bull. Geol. Soc. America, 81, 2009-2020, 1970.

Etchecopar, A., A plane kinematic model of progressive deformation in a polycrystalline aggregate, Tectonophysics, 39, 121-139, 1977.

Frey, I., Gefuge- und Metamorphosenuntersuchungen am Plattengneiss der zentralen Koralpe, W. Steiermark, Diss. Math.-Naturwiss. Fak. Univ. Wien, Austria, 1984.

Garcia Celma, A., Domainal and fabric heterogeneities in the Cap de Creus quartz mylonites, J. Structural Geology, 4, 443-455, 1982.

Garcia Celma, A., C-axis and shape fabrics in quartz mylonites of Cap de Creus (Spain): Their properties and development, Proefschrift, 130 pp., Rijksuniversiteit Utrecht, Utrecht, Holland, 1983.

Green, H. W., D. T. Griggs, and J. M. Christie, Syntectonic and annealing recrystallization of finegrained quartz aggregates, in Experimental and Natural Rock Deformation, edited by W. Paulitsch, pp. 272-335, Springer-Verlag, Heidelberg, 1970.

Groves, G. W., and A. Kelly, Independent slip systems in crystals, Phil. Mag., 8, 877-888, 1963.

Kamb, W. B., Theory of preferred orientation development by crystallization under stress, J. of Geology, 67, 153-170, 1959.

Kamb, W. B., The thermodynamical theory of non-hydrostatically stressed solids, J. Geophys. Res., 66, 259-271, 1961.

Kerrich, R., and J. Starkey, Chemical removal of feldspars and layer silicates from quartz bearing rocks for X-ray petrofabric studies, American Mineral., 64, 452, 1979.

Laurent, P., and A. Etchecopar, Mise en évidence à l'aide de la fabrique du quartz d'un cisaillement simple à déversement ouest dans le massif de Dora Maira (Alpes Occidentales), Bull. Soc. géol. France, 18, 1387-1393, 1976.

Law, R. D., M. Casey, and R. J. Knipe, The kinematic and tectonic significance of microstructure and crystallographic fabrics within quartz mylonites from the Assynt and Eriboll regions of the Moine Thrust Zone, North-west Scotland, Phil. Trans. R. Soc. Edinburgh, in press.

Law, R. D., R. J. Knipe, and H. Dayan, Strain path partitioning within thrust sheets: microstructural and petrofabric evidence from the Moine Thrust Zone at Loch Eriboll, Northwest Scotland, J. Structural Geology, 6, 477-497, 1984.

Linker, M. F., S. H. Kirby, A. Ord, and J. M. Christie, Effects of compression direction on the plasticity and rheology of hydrolytically weakened synthetic quartz crystals at atmospheric pressure, J. Geophys. Res., 89, B6, 4241-4255, 1984.

Lister, G. S., Discussion: Crossed girdle c-axis fabrics in quartzites plastically deformed by plane strain and progressive simple shear, Tectonophysics, 39, 51-54, 1977.

Lister, G. S., A vorticity equation for lattice reorientation during plastic deformation, Tectonophysics, 82, 351-366, 1982.

Lister, G. S., and U. F. Dornsiepen, Fabric transitions in the Saxony Granulite Terrain, J. Structural Geology, 4, 81-92, 1982.

Lister, G. S., and B. E. Hobbs, The simulation of fabric development during plastic deformation and its application to quartzite: the influence of deformation history, J. Structural Geology, 2, 355-370, 1980.

Lister, G. S., and M. S. Paterson, The simulation of fabric development during plastic deformation and its application to quartzite: fabric transitions, J. Structural Geology, 1, 99-115, 1979.

Lister, G. S., and P. F. Williams, Fabric development in shear zones: theoretical controls and observed phenomena, J. Structural Geology, 1, 283-297, 1979.

Lister, G. S., and P. F. Williams, The partitioning of deformation in flowing rock masses, Tectonophysics, 92, 1-33, 1983.

Lister, G. S., M. S. Paterson, and B. E. Hobbs, The simulation of fabric development in plastic deformation and its application to quartzite: the model, Tectonophysics, 45, 107-158, 1978.

Mancktelow, N. S., The Simplon Line: a major displacement zone in the Western Lepontine Alps, Eclogae, geol. Helv., in press.

Marjoribanks, R. W., The relation between microfabric and strain in a progressively deformed quartzite sequence from Central Australia, Tectonophysics, 32, 269-293, 1976.

Paterson, M. S., The ductility of rocks, in Physics of Strength and Plasticity, edited by A. S. Argon, pp. 377-392, The M. I. T. Press, Cambridge, Mass., 1969.

Paterson, M. S., Nonhydrostatic thermodynamics and its geological applications, Rev. Geoph. Space Phys., 11, 355-389, 1973.

Paterson, M. S., and L. E. Weiss, Symmetry concepts in the structural analysis of deformed rocks, Bull. Geol. Soc. America, 72, 841-882, 1961.

Poirier, J. P., and M. Guillopé, Deformation induced recrystallization of minerals, Bull. Minéral., 102, 67-74, 1979.

Riekels, L. M., and D. W. Baker, The origin of the double maximum pattern of optic axes in quartzite mylonite, J. of Geology, 85, 1-14, 1977.

Sander, B., An introduction to the study of fabrics of geological bodies, Engl. Transl., 641 pp., Pergamon Press, Oxford, 1970.

Schmid, S. M., Microfabric studies as indicators of deformation mechanisms and flow laws

operative in Mountain Building, in Mountain Building Processes, edited by K. J. Hsü, pp. 95-110, Academic Press, London, 1982.

Schmid, S. M., M. Casey, and J. Starkey, The microfabric of calcite tectonites from the Helvetic Nappes (Swiss Alps), in: Thrust and Nappe Tectonics, edited by K. R. McClay and N. J. Price, Geol. Soc. Spec. Public., 9, 151-158, 1981a.

Schmid, S. M., M. Casey, and J. Starkey, An illustration of the advantages of a complete texture analysis described by the orientation distribution function (ODF) using quartz pole figure data, Tectonophysics, 78, 101-117, 1981b.

Siddans, A. W. B., Deformed rocks and their textures, Phil. Trans. R. Soc. London, A283, 43-54, 1976.

Simpson, C., Oblique girdle orientation patterns of quartz c-axis patterns from a shear zone in the basement core of the Maggia Nappe, Ticino, Switzerland, J. Structural Geology, 2, 243-247, 1980.

Simpson, C., Displacement and strain patterns from naturally occurring shear zone terminations, J. Structural Geology, 5, 497-506, 1983.

Simpson, C., and S. M. Schmid, An evaluation of criteria to deduce the sense of movement in sheared rocks, Bull. Geol. Soc. America, 94, 1281-1288, 1983.

Simpson, C., J. Carreras, and M. Losantos, Inhomogeneous deformation in Roses granodiorite, N. E. Spain, Acta Geol. Hispaña, 4, 219-226, 1982.

Smith, G. S., and L. E. Alexander, Refinement of the atomic parameters of alpha-quartz, Acta Cryst., 16, 462-471, 1963.

Starkey, J., Petrofabric analysis of Saxony Granulites by optical and X-ray diffraction methods, Tectonophysics, 58, 201-219, 1979.

Sylvester, A. G., and J. M. Christie, The origin of crossed girdle orientations of optic axes in deformed quartzites, J. of Geology, 76, 571-580, 1968.

Tullis, J., and T. Tullis, Preferred orientation of quartz produced by mechanical Dauphiné twinning: thermodynamics and axial experiments, in Flow and Fracture of Rocks, American Geophys. Union Monograph, 16, 62-82, 1972.

Tullis, J., J. M. Christie, and D. T. Griggs, Microstructures and preferred orientations of experimentally deformed quartzites, Bull. Geol. Soc. America, 84, 297-314, 1973.

White, S. H., S. E. Burrows, and J. Carreras, Textural and microstructural development in a naturally deformed quartzite: a metallurgical approach, Proceedings of the 5th International Congress on the Texture of Materials, 2, pp. 211-220, Springer Verlag, Berlin, 1978.

Wilson, C. J. L., Preferred orientation in quartz ribbon mylonites, Bull. Geol. Soc. America, 86, 968-974, 1975.